Arch. Metall. Mater. **63** (2018), 3, 1179-1200

DOI: 10.24425/123791

T. RAMKUMAR*#, P. NARAYANASAMY***, M. SELVAKUMAR**, P. BALASUNDAR****

EFFECT OF B_4C REINFORCEMENT ON THE DRY SLIDING WEAR BEHAVIOUR OF Ti-6Al-4V/B_4C SINTERED COMPOSITES USING RESPONSE SURFACE METHODOLOGY

The present investigation has been made to assess the influence of B_4C reinforced with Ti-6Al-4V matrix prepared by powder metallurgy route. High energy ball milling was used to prepare the composites. Cylindrical preforms were prepared using suitable die set assembly. The green preforms were sintered in the muffle furnace at 900°C for 1 h. Further the preforms were cooled inside the furnace till the room temperature has attained. SEM with EDS mapping analysis was used to evaluate the morphology and elemental confirmation of the prepared composite. The density and hardness of the samples are determined using Archimedes principle and Rockwell hardness testing machine. The wear resistance of the samples was determined by employing a pin on disc apparatus. The hardness of the composites (Ti-6Al-4V /10B_4C) was increased while comparing to the base material (Ti-6Al-4V) which is attributed to the presence of hard ceramic phase. Response Surface Methodology (RSM) five level central composite design approach was accustomed and it minimised the amount of experimental conditions and developed mathematical models among the key process parameters namely wt. % of B_4C, applied load and sliding distances to forecast the abrasive response of Specific Wear Rate (SWR) and Coefficient of Friction (CoF). Analysis of variance was used to check the validity of the developed model. The optimum parameters of specific wear rate and coefficient of friction were identified.

Keywords: Ti-6Al-4V; B_4C; powder metallurgy; dry sliding wear; response surface methodology

Highlights:

- Prepared Ti-6Al-4V /B_4C composites by powder metallurgy technique.
- Composites have been prepared to Relative density of ≥85%.
- Specific wear rate, coefficient of friction and hardness were enriched because of the reinforcement of hard ceramic particles.
- The optimum parameters of specific wear rate and coefficient of friction were identified, using Response Surface Methodology.

1. Introduction

Design and development of ceramic particle reinforced titanium matrix composites (TMCs) have been extensively studied, due to their superior wear resistance and increased mechanical properties when compared to unreinforced titanium alloys [1]. Among the titanium based alloys, aluminium and vanadium reinforcement (Ti-6Al-4V) is used in aircraft and turbines due to its heat treatment ability, adequate mechanical strength, and good corrosion resistance [2]. Application of titanium is limited because of some crucial factors such as poor wear resistance and relatively low hardness [3]. Incorporation of alloying elements, aluminium and vanadium to the titanium matrix improves the grain refinement and rust resistance [4]. Several researchers studied [2-5] and was concluded that, due to the incorporation of hard ceramic particles like B_4C, TiB_2, TiC, W, Al_2O_3 into the metal matrix improved the wear resistance of the composites. The predominant factors that influence the wear behaviour of the TMCs are classified into several categories such as size, shape, distribution in the matrix, the weight percentage (intrinsic factors) and applied load, sliding velocity and sliding distance (extrinsic factors). Mohammad Sharifi et al. [6] reported that, B_4C particles were more effective than other ceramic particles for the improvement of wear resistance of metal matrix composites due to its excellent hardness. Even though there are several techniques to fabricate the titanium based composites such as thermal spraying, hot pressing, hot extrusion and stir casting [7], the most suitable technique for even dispersion of reinforcement in the matrix and grain refinement was Powder Metallurgy (P/M) [8-10] Technique. Moreover, many researchers have made an attempt to increase the ultimate strength, compressive strength and ductility of the titanium matrix composites [11-15]. Math-

* DEPARTMENT OF MECHANICAL ENGINEERING, DR.MAHALINGAM COLLEGE OF ENGINEERING AND TECHNOLOGY, POLLACHI, TAMILNADU, INDIA
** DEPARTMENT OF AUTOMOBILE ENGINEERING, DR.MAHALINGAM COLLEGE OF ENGINEERING AND TECHNOLOGY, POLLACHI, TAMILNADU, INDIA
*** DEPARTMENT OF MECHANICAL ENGINEERING, KAMARAJ COLLEGE OF ENGINEERING AND TECHNOLOGY, VIRUDHUNAGAR, TAMILNADU, INDIA
**** DEPARTMENT OF MECHANICAL ENGINEERING, RAJALAKSHMI INSTITUTE OF TECHNOLOGY, CHENNAI TAMILNADU, INDIA

Corresponding author: ramkimech89@gmail.com

ematical models of Specific wear rate and Coefficient of friction properties of the composites were established using Response Surface Methodology (RSM). RSM is a useful method that is extensively employed to understand the relationships between the factors and the responses by modelling the process. It is a collective of statistical experimental design, regression modelling and optimization. Several studies have reported the tribological properties using RSM [16]. Vettivel et al [17] successfully developed a wear model for the relationship of wt. % of tungsten, applied load, sintering temperature and sliding distances on dry wear properties of Cu-W composites using RSM. Yang et al [18] reported that the wear model for the relationship of applied load, sliding speed and sliding distances on dry sliding wear conditions of fibre reinforced hybrid composites.

Literatures reporting on dry sliding wear behaviours of TMCs fabricated through P/M are limited. It is therefore, proposed to undertake a study to analyse the effect of B_4C reinforced Ti-6Al-4V matrix alloy on the dry sliding wear behaviour prepared through P/M method. Characterization of the TMC specimens has been investigated by using SEM with EDS mapping. Tribological properties of the TMC was evaluated by using pin-on-disc wear testing machine. Further, RSM model was used to exploring the independent of the process parameters and second order quadratic model for the prediction of results where the data was attained by conducting the wear test experiments. In addition to find the optimum parameters of specific wear rate and coefficient of friction using response surface methodology.

2.0. Experimentation

2.1. Materials

Ti, Al, V and B_4C powders were used in the present investigation. They were purchased to ≥99.9% purity from M/s. Alfa Aesar, USA and M/s. Sigma Aldrich, Germany. The powders were mixed on weight basis to attain the required composition. Fig. 1a-d showed the titanium, aluminium, vanadium and boron carbide powders before milling. The purchased titanium, aluminium, vanadium and boron carbide have Hexagonal Closed Pack (HCP), Face Centred Cubic (FCC), Body Centred Cubic (BCC) and rhombohedral structure respectively.

2.2. Powder Milling

Elemental powders of Ti, Al, V and B_4C of less than 44 μm in size are milled separately by using an inert ball milling process (Fritsch, Germany- Pulverisette-6). Tungsten Carbide (WC) balls and WC container are used to mill the powders with a desired

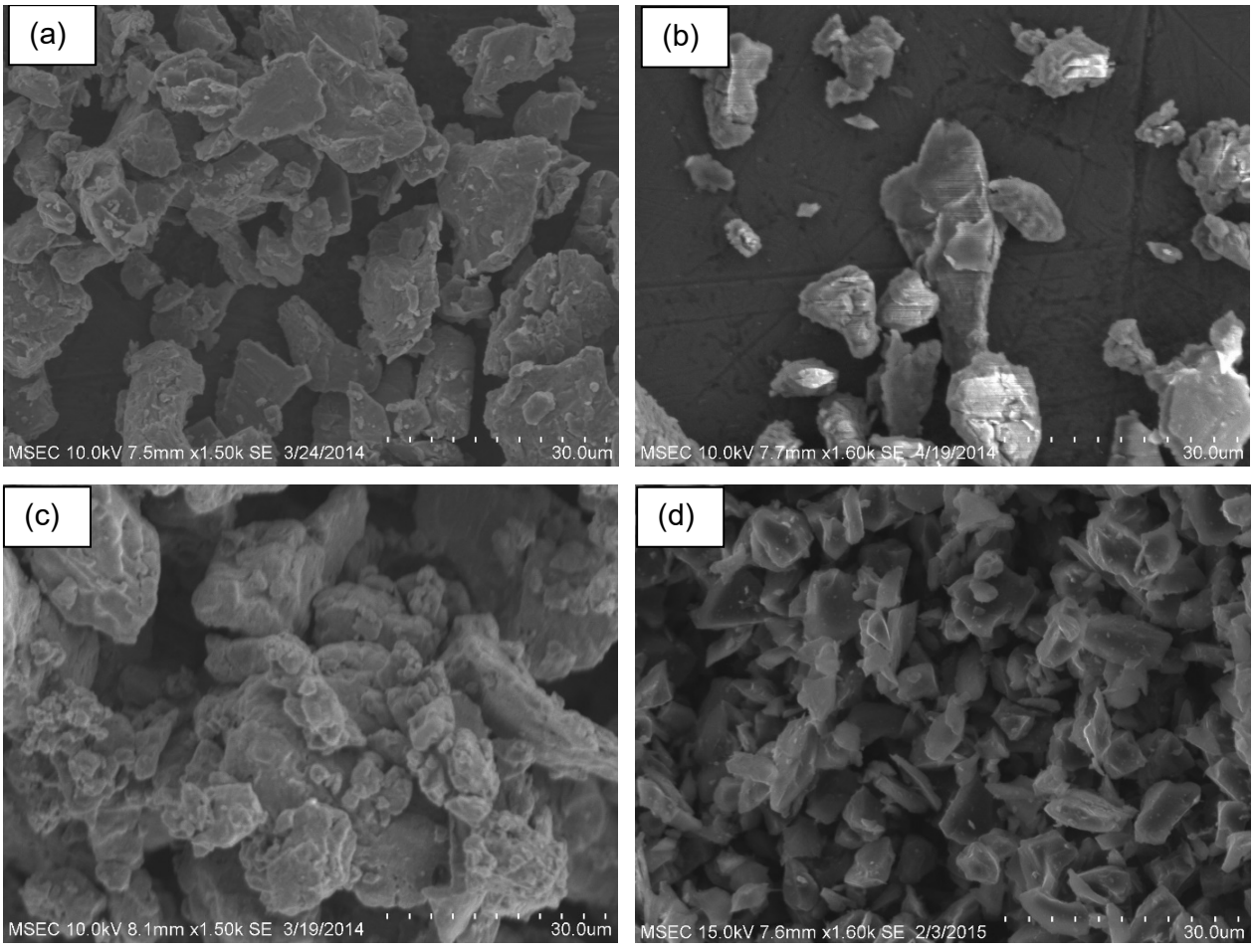

Fig. 1a-d. SEM images of the received titanium, aluminium, vanadium and boron carbide powders

ball to powder ratio. WC has more abrasion resistance than the powders, and hence is not mingled with any of the milled constituents. Milling was carried out at constant speed of 300 rpm in wet medium. Wet milling with inert gas circulated environment was also used to avoid oxidation, high temperature development etc. The organic compound toluene (C_6H_5-CH_3) were filled in the ball mill chamber in adequate quantity, and its level is frequently checked in each interval. The milling experiments were interrupted at a regular interval of 0.25 h for cooling. Desired milling time was required to attain ≤500 nm of final metallic particles. B_4C can be further milled to lower particle size to the order of ≤200 nm. Fig. 2a shows the SEM image of the titanium powder particles after 40 h of milling. It was in flattened shape and is reduced to ≤500 nm. Fig. 2b shows the SEM image of the aluminium powder after milling for 55 h. The spherical form was transferred to sharp flattened shape and reduced to ≤500 nm after desired milling. Further, Fig. 2c shows the SEM image of the vanadium powder particles after milling for 38 h. It was in hexagonal shape and size reduced to ≤500 nm. Fig. 2(d) shows the SEM image of the boron carbide powder particles after milling for 50 h. It was in spherical shape and is reduced to ≤200 nm.

Particle size analysis is the most important characterization technique to analyze the nano scale powders. The particle size analyzer (ZETASIZER, Malvern-UK, Model: Nano-ZS90) was used to examine the exact size of the powders. For particle size analysis 0.001 g of powder was dispersed in the 50 ml of water, and then the powder was ultra-sonicated for 15 min. Hence, the powders were evenly dispersed in the water. Further, the particle sizes were recorded by using particle size analyzer. Fig. 3a-d shows the particle sizes of titanium, aluminium, vanadium and boron carbide powders, measured using particle size analyser. The peaks confirmed that all the powders are in 100-200 nm range [19].

2.3. Preparation and characterization of composites

The desired powders were mixed in the weight ratio of 90:6:4 for Ti: Al: V respectively to attain Ti-6Al-4V matrix. However, while preparing Ti-6Al-4V /B_4C composite, the reinforced particle (B_4C) is blended with Ti powder with weight percentage of (2-12%) of B_4C by retaining other elements as constant (Al, V). Further the pre mixed powers were blended in the plantery ball mill for 1 h.

Fig. 4a-d shows the micrograph of various weight percentage (2-12%) of the boron carbide present in the Ti-6Al-4V matrix. It clearly shows that all the particles were uniformly distributed in the composites.

Blended powder mixture was compacted in the suitable die set assembly on a compression testing machine. Compacting pressure was applied gradually to reach 2.5 GPa for all specimens. MoS_2 was used as a lubricant for the die set assembly. The compacted specimens were sintered in the muffle furnace

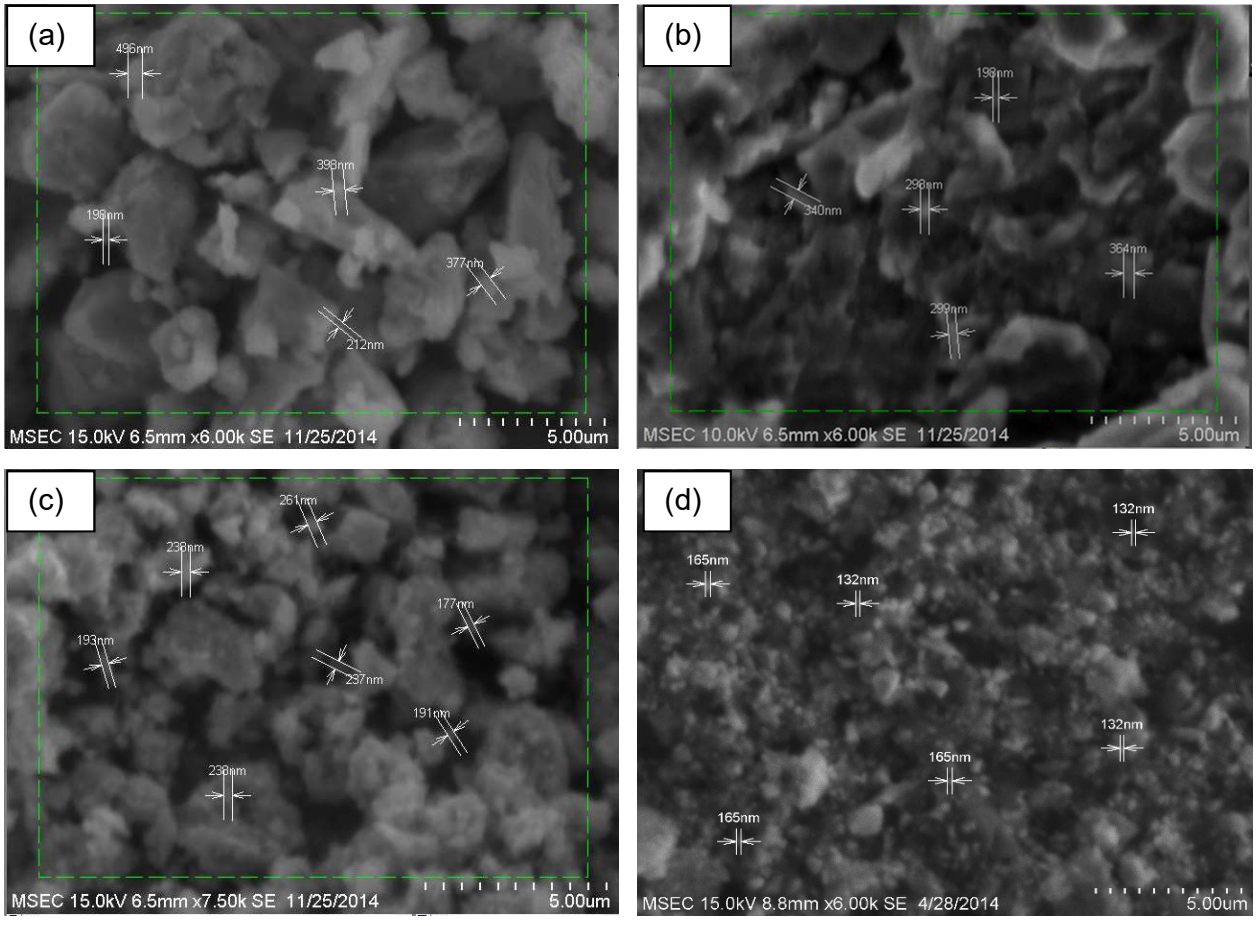

Fig. 2a-d. SEM images of the titanium, aluminium, vanadium and boron carbide powders after ball milling

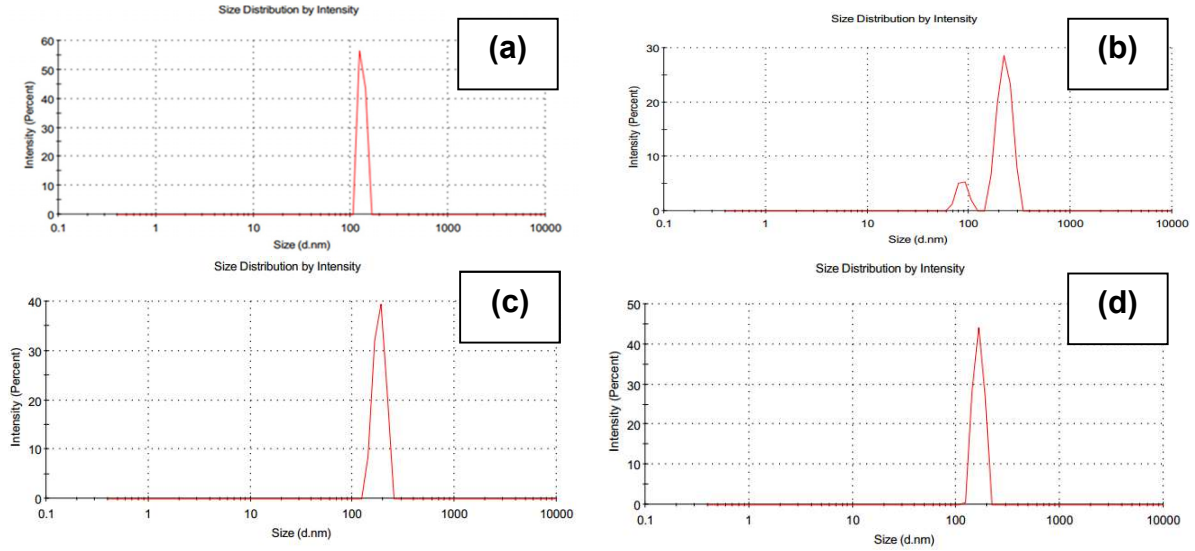

Fig. 3a-d. Particle size analysis of (a) Titanium, (b) Aluminium, (c) Vanadium and (d) Boron carbide

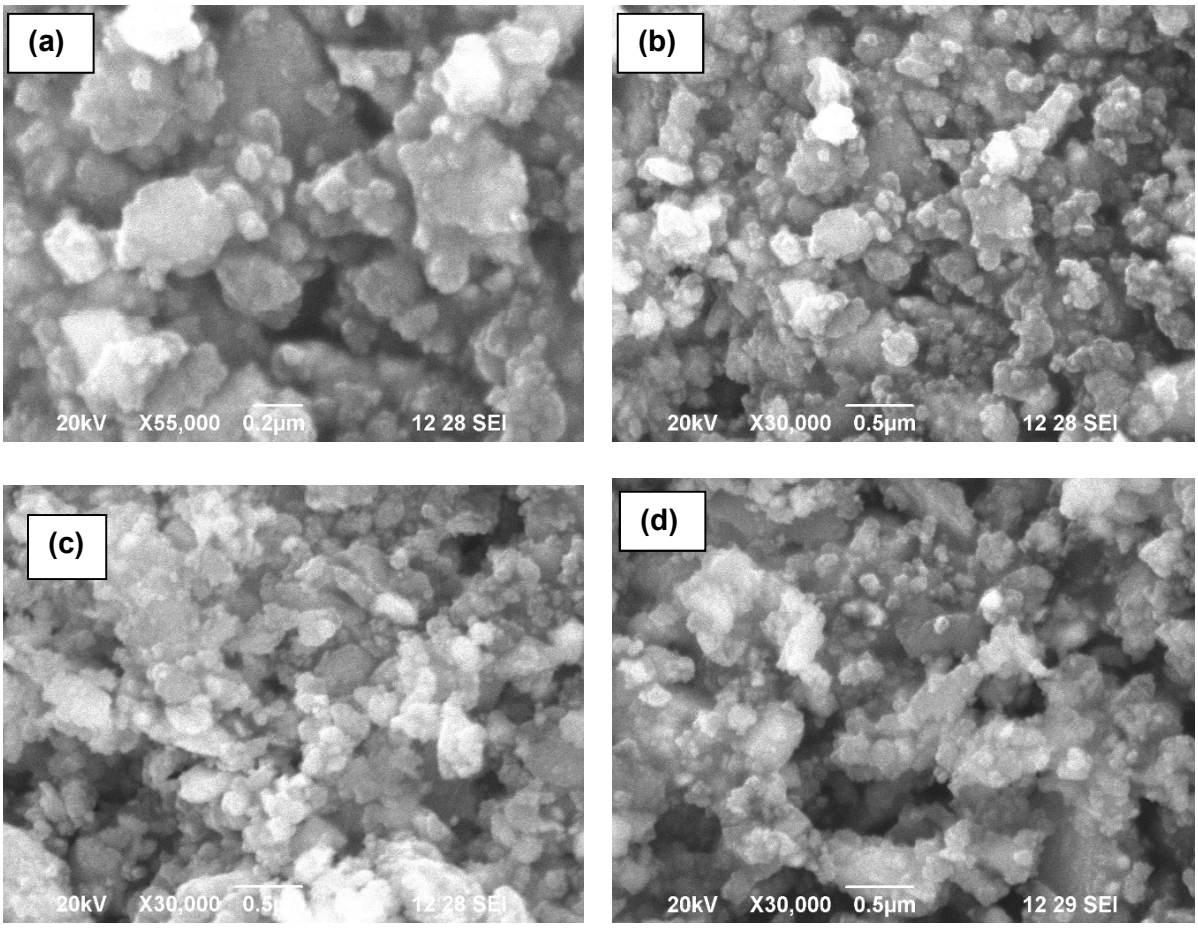

Fig. 4a-f. SEM micrograph of the various wt. % of powder samples (a) Ti-6Al-4V (b) Ti-6Al-4V /4B_4C (c) Ti-6Al-4V /8B_4C (d) Ti-6Al-4V /12B_4C

at 900°C for a holding period of 1 h, and then the preforms were subsequently cooled inside the furnace itself, until the room temperature was obtained [20]. After the completion of sintering, the preforms were polished using emery paper of various grit sizes such as 800, 1000, 1200 µm. The sintered composite samples were polished mechanically and etched chemically using Kroll's reagent (a mixture of 10 ml HF, 5 ml HNO_3 and 85 ml H_2O). Then the microstructures of the samples were observed using optical microscopy. SEM micrograph mapping of elements were recorded by electron scanning electron microscopy, the chemical composition of elements was observed by energy-dispersive spectroscopy. The theoretical density of the composites was measured using Archimedes principle. The average densities of the composites were ≥85%. The hardness test was carried out

by using a Rockwell hardness testing machine with a diamond indenter and 150 kgf load for 10 s using C scale. The measurement of hardness was taken at three different places on each sample to find the average value. Before testing, the samples were polished with various sizes of grit/emery papers.

2.4. Microstructural analysis

Figure 5a shows the microstructures of the sintered Ti-6Al-4V matrix alloy. Figure 5b-g shows the microstructures of sintered Ti-6Al-4V – B_4C composites. A micrograph of B_4C

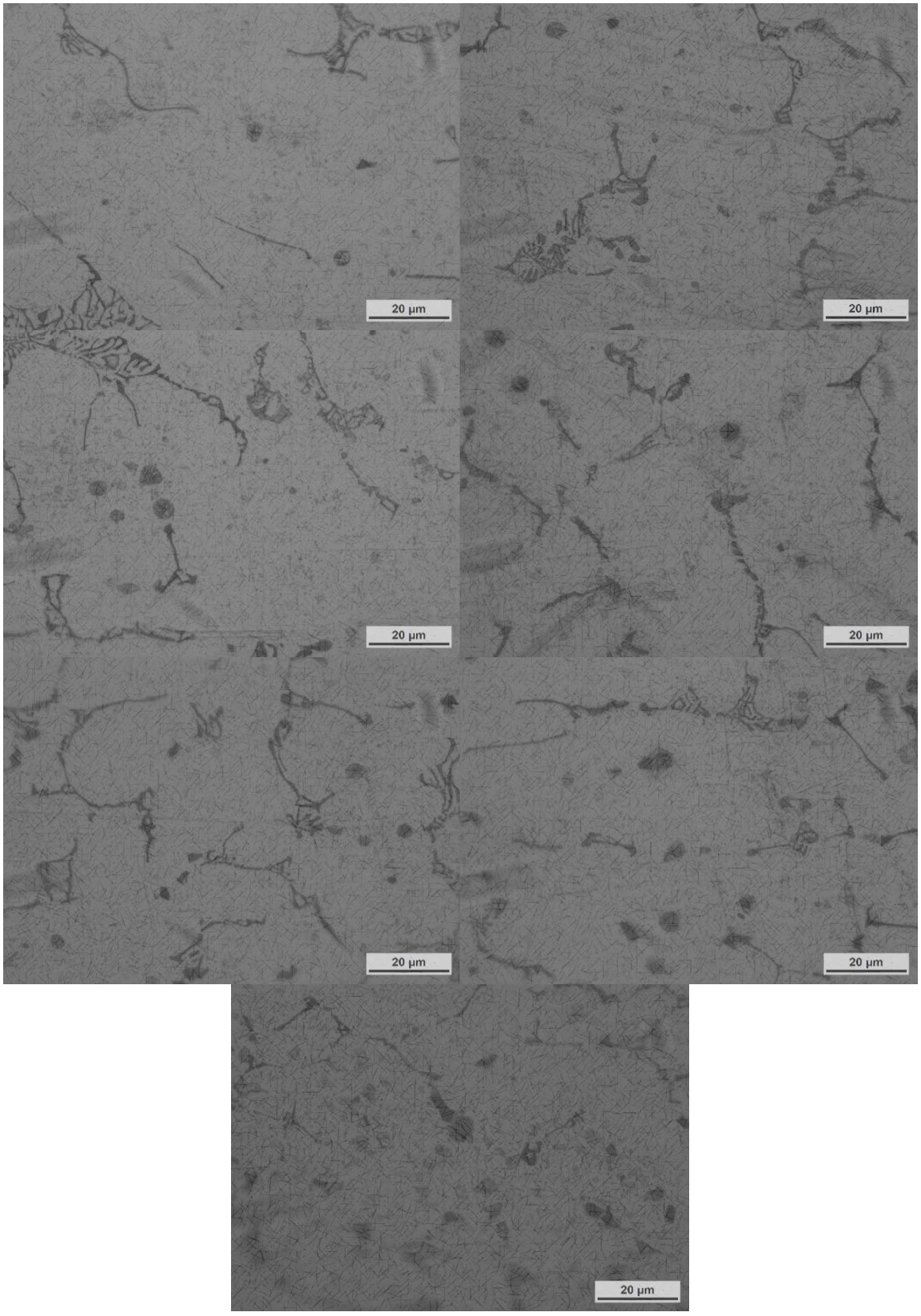

Fig. 5. Microstructural analysis of composites at various wt. % of B_4C addition

reinforced composite clearly depicts good interface bonding between Ti-6Al-4V matrix and B_4C reinforcement particles. B_4C particles are uniformly distributed in the entire Ti-6Al-4V matrix. Among them, Ti-6Al-4V /10 B_4C composite is relatively more homogenous along with the matrix compared with other composites, as shown in Fig. 5f. The reinforcements add a strong interface and good wettability in Ti-6Al-4V matrix and show no macro porosity, particularly at the grain boundaries of interface. There is no perceptibility in bonded or delamination interface detected between the matrix and reinforcement particles. In addition, the absence of pores and cracks can also be experienced in the micrographs.

2.5. SEM with EDS mapping analysis

SEM with EDS mapping analysis of Ti-6Al-4V matrix and Ti-6Al-4V /B_4C composites microstructure after sintering was recorded using Burker equipment with accelerating voltage of 0.2 to 30 kV, probe current of 0.5 µA to 5 µA and energy dispersive spectrometer as a detector at Kalasalingam University, Tamil Nadu and India.

Fig. 6 shows that SEM with EDS mapping of Ti-6Al-4V matrix. Figure 6 reveals that the elements such as titanium, aluminium and vanadium particle were observed. From the spectrum it has been asserted that Al and V has successfully incorporated in the titanium (Ti-6Al-4V). From the EDS analysis, it is also

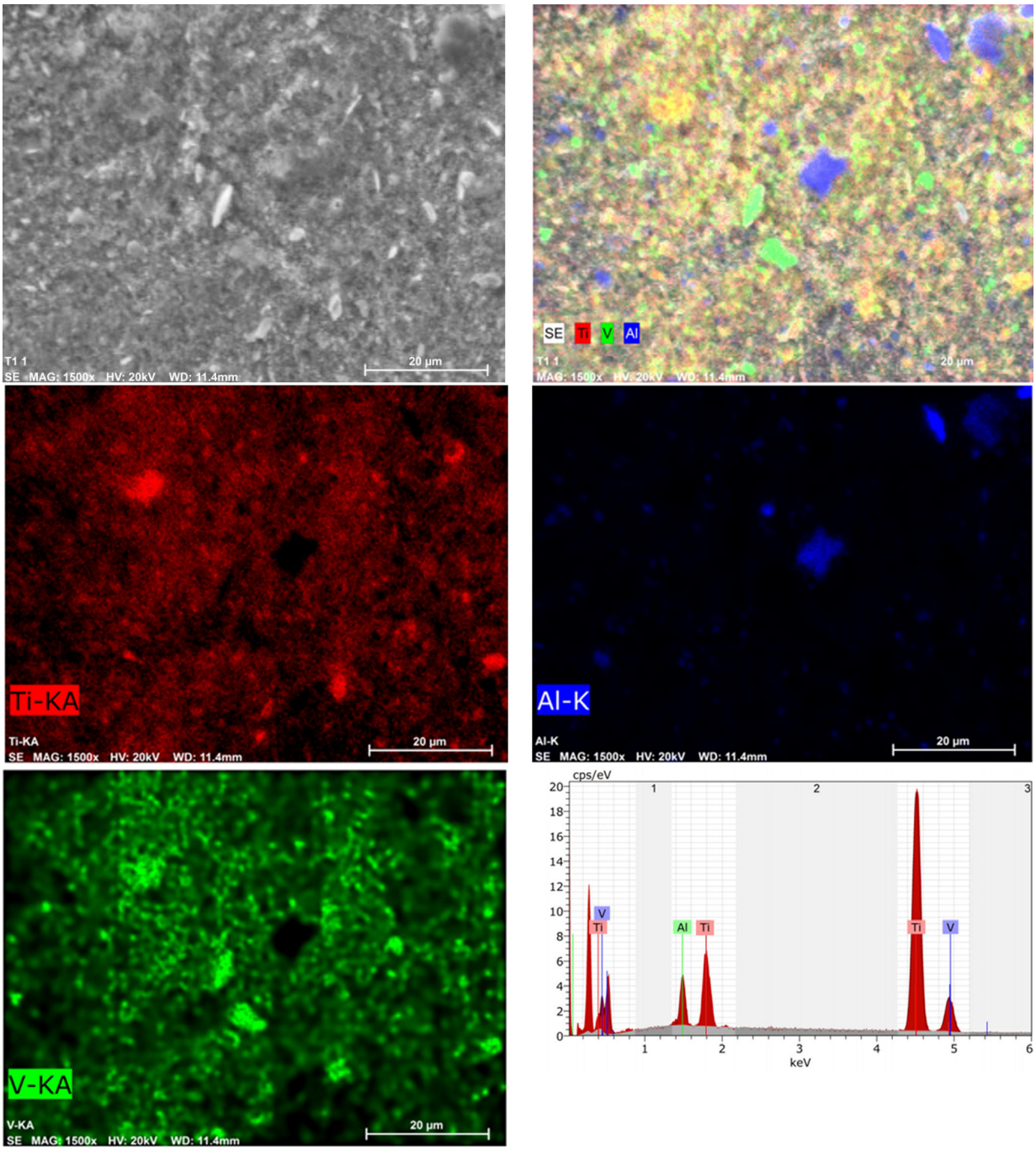

Fig. 6. SEM with EDS mapping of Ti- 6Al-4V matrix

inferred that high intensity, medium intensity and low intensity peaks represent titanium, aluminium and vanadium respectively. The map overlay of all three elements shows the presence of Ti (red), Al (Violet) and V (green) respectively. It is also inferred that there are some areas where those elements are not combinations with any of the others.

Figure 7 shows that SEM with EDS mapping of Ti-6Al-4V /B_4C composites. From the figure it reveals that the secondary

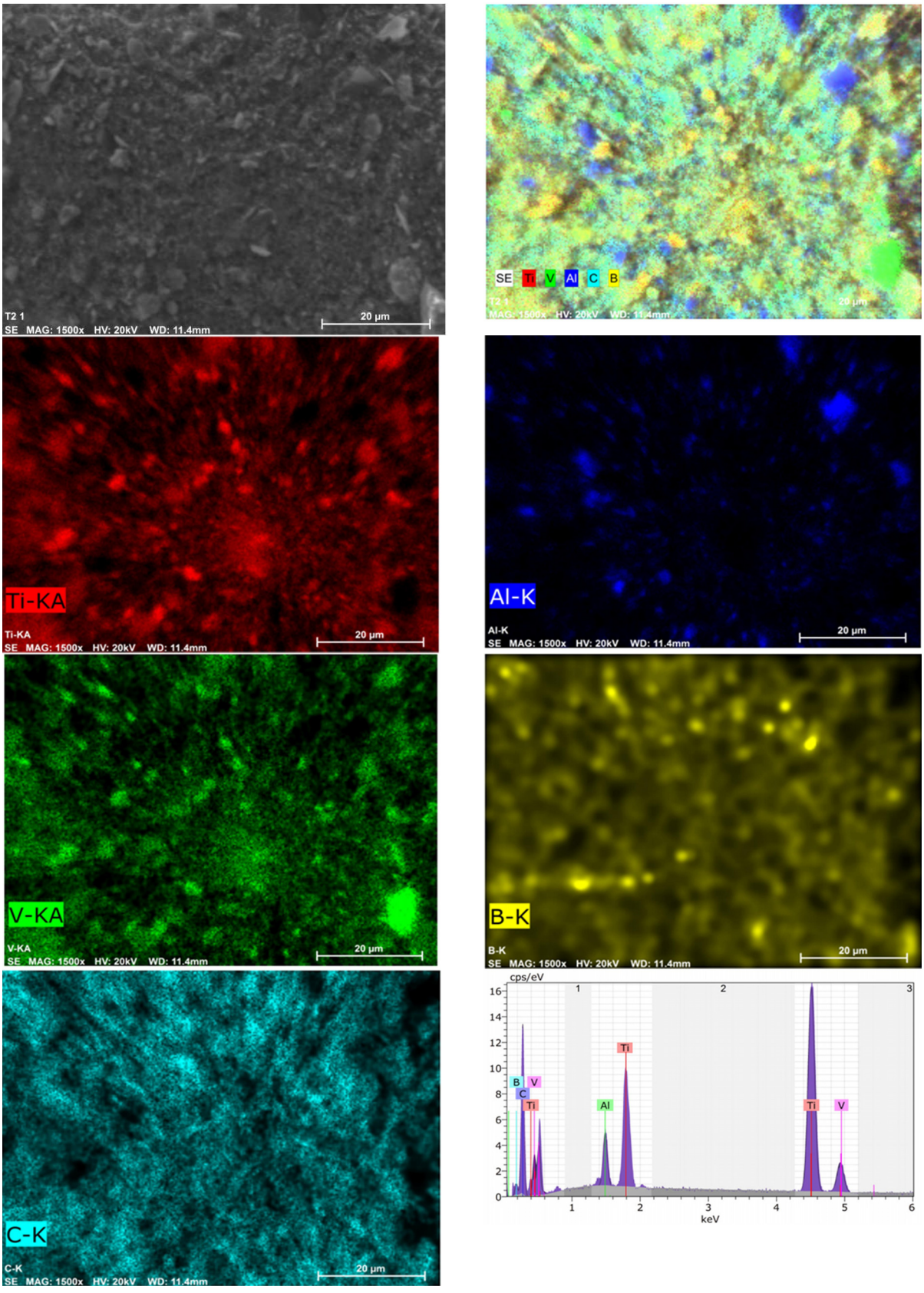

Fig. 7. SEM with EDS mapping of Ti-6Al-4V matrix and Ti-6Al-4V / B_4C composite

particle (B_4C) has been evenly distributed in the matrix material after sintering. It has been ascertained the corresponding EDS analysis. Furthermore, no oxide peak was observed in the EDS spectrum, which confirms that no solid-state reactions took place between Ti-6Al-4V and B_4C during sintering. The map overlay of all five elements shows where the Ti (red), Al (violet), V (green), boron (yellow) and carbon (blue).

2.6. Density Measurement

The theoretical densities of the composite preforms were calculated by using the rule of mixture. The actual density of the composites was calculated by Archimedes principle and is shown in Table 1. The relative density has been calculated using the ratio of the actual density to theoretical density. All the composites possess relative density of more than ≥85% and it illustrates that the porosity of the composites was also reduced by the addition of B_4C content. This is due to less particle size of B_4C with Ti-6Al-4V matrix for the same compaction pressure of 2.5 GPa. The details of the Ti-6Al-4V / B_4C composite density details are shown in Table 1.

TABLE 1

Density measurement of the prepared composites

B_4C addition (wt.%)	Theoretical density (g/cm^3)	Actual density (g/cm^3)	Relative density	Porosity (%)	Hardness (VHN)
0	4.47	3.98	0.89	0.11	290
2	4.43	3.99	0.90	0.10	340
4	4.39	3.95	0.90	0.10	380
6	4.35	3.96	0.91	0.09	400
8	4.32	3.93	0.91	0.09	460
10	4.27	3.93	0.92	0.08	520
12	4.31	3.99	0.93	0.09	440

2.7. Hardness analysis

Table 1 provides the variations of hardness of base metal and composite materials, namely Ti-6Al-4V, Ti-6Al-4V /12B_4C with an increment of 2% of B_4C. This shows there is a continuous improvement of hardness for the addition of B_4C with base Ti-6Al-4V matrix. Further, the result shows that Ti-6Al-4V /10B_4C displays higher hardness. This can be attributed to the addition of B_4C ceramic particle that has been uniformly distributed in the matrix material. By adding the B_4C particle into the base material, the hardness has been significantly increased. Moreover, the hardness of the composites has twice to that of the base material (Ti-6Al-4V). It can be further deduced that the hardness of all the composites was significantly greater than the base material because of high volume fraction of the ceramic B_4C particles in the matrix (Ti-6Al-4V). While reinforcing 12 Wt. % B_4C the hardness was decreased because of the agglomeration of the secondary phase [20].

2.8. Wear test

Wear test was conducted using a Pin- on- Disc testing machine (DUCOM, Bangalore; Model: TR-20LE-PHM-400). The counter disc is made up of EN 31 steel hardened to 60 HRC. It's high measure of hardness with abrasion resistance and quite often used for wear resisting machine constituents leads to the ultimate choice for counterpart disc material. The samples were prepared as per the ASTM: G99-05 standard. The samples were in cylindrical form with 10 mm diameter, and 30 mm height. The contact surface of the specimens was polished by using various grit/emery papers such as 800, 1000, 1200 microns. The wear test was carried out at an applied load of 10 N, 15 N, 20 N, 25 N and 30 N, and then the sliding distance was varied to 1000 m, 1400 m, 1800 m and 2200 m with constant velocity of 3.14 m/s. The test was conducted at room temperature. After wear test, the samples were cleaned with acetone, and then the wear resistance was measured in terms of weight loss of the tested specimens using an electronic digital balance machine with an accuracy of ±0.001 mg. By using the calculated weight loss in wear test, it is converted into specific wear rate as per the Eq. (1). The frictional force is measured by the wear testing machine during the experiment and it is converted into coefficient of friction (CoF) using Eq. (2) [17].

$$\left(\begin{matrix}Specific\cdot wear\cdot\\ rate\cdot\left(\dfrac{\mathrm{mm}^3}{\mathrm{N}\times\mathrm{m}}\right)\end{matrix}\right)=\frac{Volume\cdot loss}{\left(\begin{matrix}Load\cdot X\cdot\\ Sliding\cdot disance\end{matrix}\right)} \tag{1}$$

$$\left(\begin{matrix}Coefficient\cdot\\ of\cdot friction\end{matrix}\right)=\frac{Frictional\cdot force}{Applied\cdot load} \tag{2}$$

The weight loss of pure Ti-6Al-4V and Ti-6Al-4V / X wt. % B_4C composites were measured and compared. Worn surface and wear debris particles were investigated using scanning electron microscope after the wear test.

3. Experimental design

Response surface methodology (RSM) is a statistical tool that are useful for modelling, analysing and predicting the process/product that affords an overall perspective of the system response with in the design space. The foremost wide-ranging applications of RSM especially in particular situations wherever several input variables probably influence some performance measure or excellence characteristic of the process. The experiments are designed based on central composites design (CCD) scheme of design of experiments (DOE). CCD is very effective experimental technique in studies involving large number of factors. A set of experimental design that can look at K factors in 'n' observations with each factor at two levels is called two level factorial design, which can prove good and efficient when a linear relationship prevails between the factors and the response. Three or higher level experiments are mandatory when

nonlinear relationship exists, which ends up with increased cost and time of testing. CCD is the most efficient method, alternative to 3 k or more factorial experimental designs. CCD can be used to study factors at five levels in reduced number of tests. In the present investigation Wt. % of B_4C (A), applied load (B) and sliding distance (C) are identified as process parameters. Specific wear rate (SWR) and coefficient of friction (CoF) are the responses. The effects of the parameters on A, B and C are tested through a collection of experiments based on standard RSM design referred to as central composite design (CCD). The response variables investigated are the SWR and CoF. For the specific input parameters, the second order polynomial equation was used to represent the response surface 'Y' is given in [21-23]

$$\text{Specific wear rate } (SWR) = f(A, B, C) \tag{3}$$

$$\text{Coefficient of friction } (CoF) = f(A, B, C) \tag{4}$$

According to the selected parameters of three factors and five levels, units and notifications of the central composite design model of RSM. Table 2 shows the factors and their levels employed in the experiments. Table 3 provides the experimental plan and the experimental results obtained. The Design Expert Software 10.1 was used to conduct the statistical analysis and to develop the mathematical models of the composites.

TABLE 2

Input levels of dry sliding wear

S. No	Parameter	Unit	Level				
			–1	**–1**	**0**	**1**	**1**
1.	A: B_4C Content	Wt. %	0	4	6	8	12
2.	B: Applied load	N	10	15	20	25	30
3.	C: Sliding distance	m	1000	1400	1800	2200	2600

TABLE 3

Actual design factors and responses accrued from RSM

Run	Std.	Reinforcement (A) Wt.%	Applied load (B) N	Sliding distance (C) m	SWR * 10^{-3} mm^3/N-m	CoF
1	14	0	0	1	0.37	0.77
2	16	0	0	0	0.43	0.78
3	10	1	0	0	0.33	0.72
4	17	0	0	0	0.43	0.78
5	2	0.5	–0.5	–0.5	0.33	0.63
6	7	–0.5	0.5	0.5	0.52	0.89
7	4	0.5	0.5	–0.5	0.4	0.725
8	8	0.5	0.5	0.5	0.43	0.8
9	12	0	1	0	0.5	0.85
10	11	0	–1	0	0.36	0.73
11	15	0	0	0	0.43	0.78
12	5	–0.5	–0.5	0.5	0.45	0.82
13	9	–1	0	0	0.52	0.9
14	18	0	0	0	0.43	0.78
15	19	0	0	0	0.43	0.78
16	1	–0.5	–0.5	–0.5	0.41	0.75
17	6	0.5	–0.5	0.5	0.38	0.73
18	20	0	0	0	0.43	0.78

3.5. Numerical modelling

All the experimental results were evaluated through RSM to frame an empirical model for the best response. The assessed response appeared to have a functional relationship only in a localized region (or) near the central point of the model. The linear and quadratic models were used to describe the mathematical relationship between the factors and responses. All the factors were evaluated at 99.5% confidence level applying fisher's F-test using RSM software package. After determining the substantial factors, the ultimate models were established using only these factors and the final mathematical models were established to estimate the specific wear rate and coefficient of friction [23]. The mathematical expressions for the specific wear rate and coefficient of friction with the coded variables like A, B and C are shown below:

$$\begin{aligned}\text{Specific wear rate } (SWR) = {} & + 0.43 - 0.048 * A + \\ & + 0.037 * B + 0.013 * C - 3.750\text{E}^{-003} * AB + \\ & + 1.250\text{E}^{-003} * AC - 3.750\text{E}^{-003} * BC + \\ & + 3.037\text{E}^{-003} A^2 + 4.804\text{E}^{-003} * B^2 - 0.020 * C^2\end{aligned} \tag{5}$$

$$\begin{aligned}\text{Coefficient of friction } (CoF) = {} & + 0.78 - 0.052 * A + \\ & + 0.038 * B + 0.037 * C + 1.875\text{E}^{-003} * AB + \\ & + 5.625\text{E}^{-003} * AC - 4.375\text{E}^{-003} * BC + \\ & + 0.011 * A^2 + 4.059\text{E}^{-003} * B^2 - 0.024 * C^2\end{aligned} \tag{6}$$

3.6. Checking of data and adequacy of model

3.6.1. Normality of the data

The normality plot of the residuals for specific wear rate and coefficient of friction is shown in Fig. 8. Fig. 8a is the normal probability plot for specific wear rate and Fig. 8(b) corresponding to the coefficient of friction that illustrates that the residuals are dropping on the straight line. This implies the errors, dispersed unremarkably.

3.6.2. Independency of the data

Independency of the info was evaluated by plotting a graph between the residuals and also the run order. Specific wear rate and coefficient of friction residual plot are shown in Fig. 9. Fig. 9a is that the residual plot for SWR and Fig. 9b corresponding CoF, that illustrates that there was no expected pattern perceived as a result of all the residues runs between –6 to 6 levels.

3.6.3. Residuals data analysis

The residual plot for specific wear rate and coefficient of friction are shown in Fig. 10. Fig. 10a-c reveals the residual plot

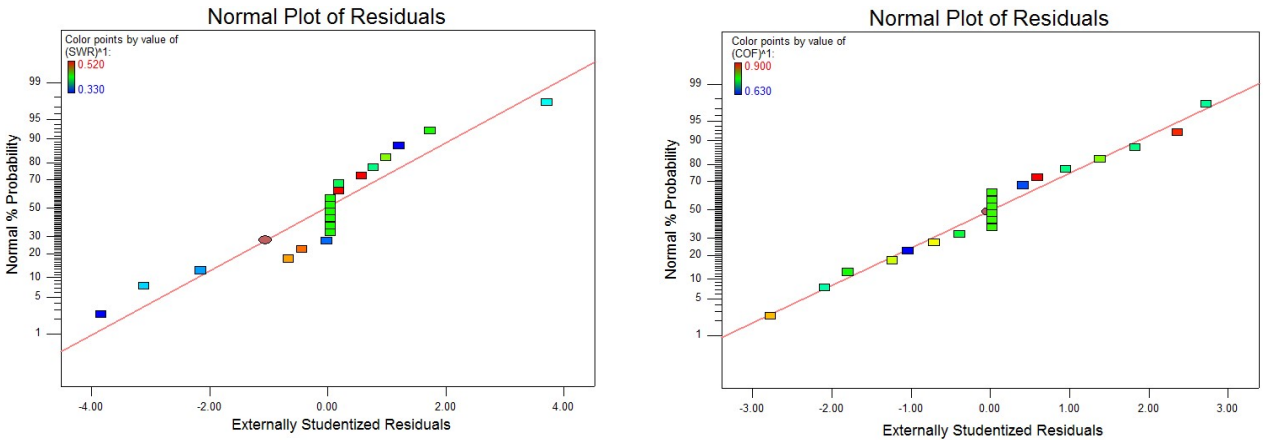

Fig. 8. Normal probability plots a) Specific wear rate and b) Coefficient of friction

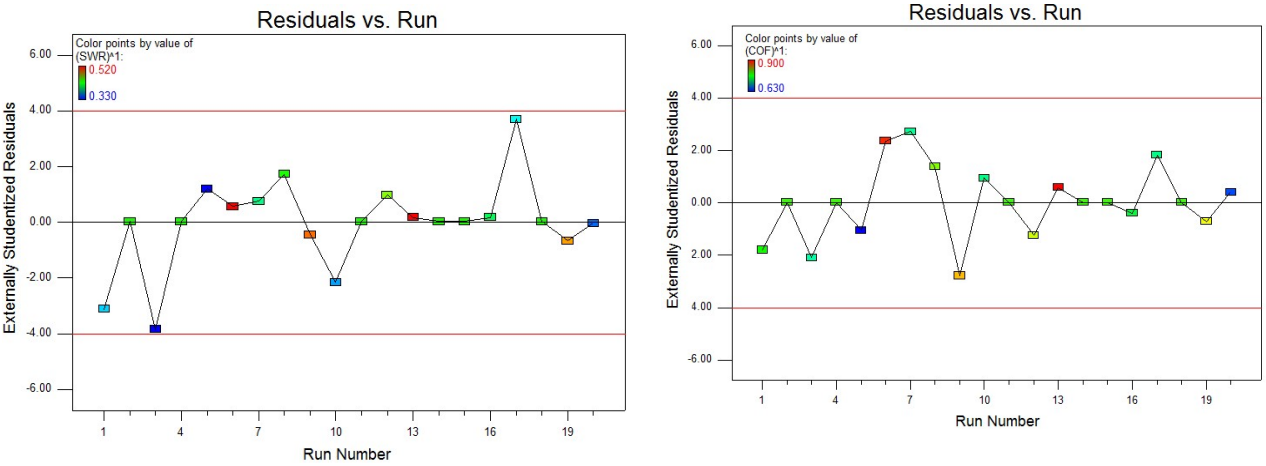

Fig. 9. Residuals plots a) Specific wear rate and b) Coefficient of friction

for SWR in terms of Wt. % of reinforcement, applied load and sliding distance and Fig. 10d-f to the coefficient of friction, that reveals that there was no predictable arrangement are seeming as a result of all the residues runs between –6 to 6 levels.

4.0. Results and discussion

4.1. Wear test analysis

4.1.1. Effect of coefficient of friction on sliding distance

Fig. 11a-d shows the change in coefficient of friction against applied loads (10-30 N) for Ti-6Al-4V base material and Ti-6Al-4V / (2-12) wt. % of B_4C composites tested at ambient temperature. While increasing the load, coefficient of friction of the contact surface increases, and also that while increasing the sliding distance, the contact pressure also decreases due to the increase in contact area [23-25]. In the initial stage of sliding, the adhesion between the specimen and the counter disc is higher, which increases the coefficient of friction. While adding the hard asperities (B_4C) into the matrix material, it reduces the friction coefficient between the composites and counter disc [26-28].

Fig. 11a-d shows the coefficient of friction for the Ti-6Al-4V matrix and Ti-6Al-4V / (0-12) wt. % of B_4C composites for 1000, 1400, 1800 and 2200 m sliding distances. It reveals that the coefficient of friction is decreased with increase in B_4C content. Similar trend was noted for other sliding distances. During sliding, the initial metal to metal contact between the specimen and counter face is higher. Hence, the huge amount of heat is generated, which increases the coefficient of friction gradually. It is also identified that using initial condition of sliding, the adhesion between the specimen and counter disc is higher and thus it increases the friction coefficient. While increasing in the B_4C content, the part of the B_4C on the sample surface increases, and therefore they act as a shielding while doing the wear test, and thus they contribute to enhance the coefficient of friction. In other words, the hard B_4C reinforcement has deeply penetrated into the soft matrix material thus increase the abrasive wear. During sliding, the B_4C can cover the wear surface and act as obstacles which decreases the coefficient of friction.

From the Fig. 11a-d it also illustrates that for 30 N load with 1000, 1400, 1800 and 2,200 m sliding distances, the coefficient of friction is varied from 0.62, 0.65, 0.72 and 0.75 respectively. It further illustrates that while increasing sliding distance, the

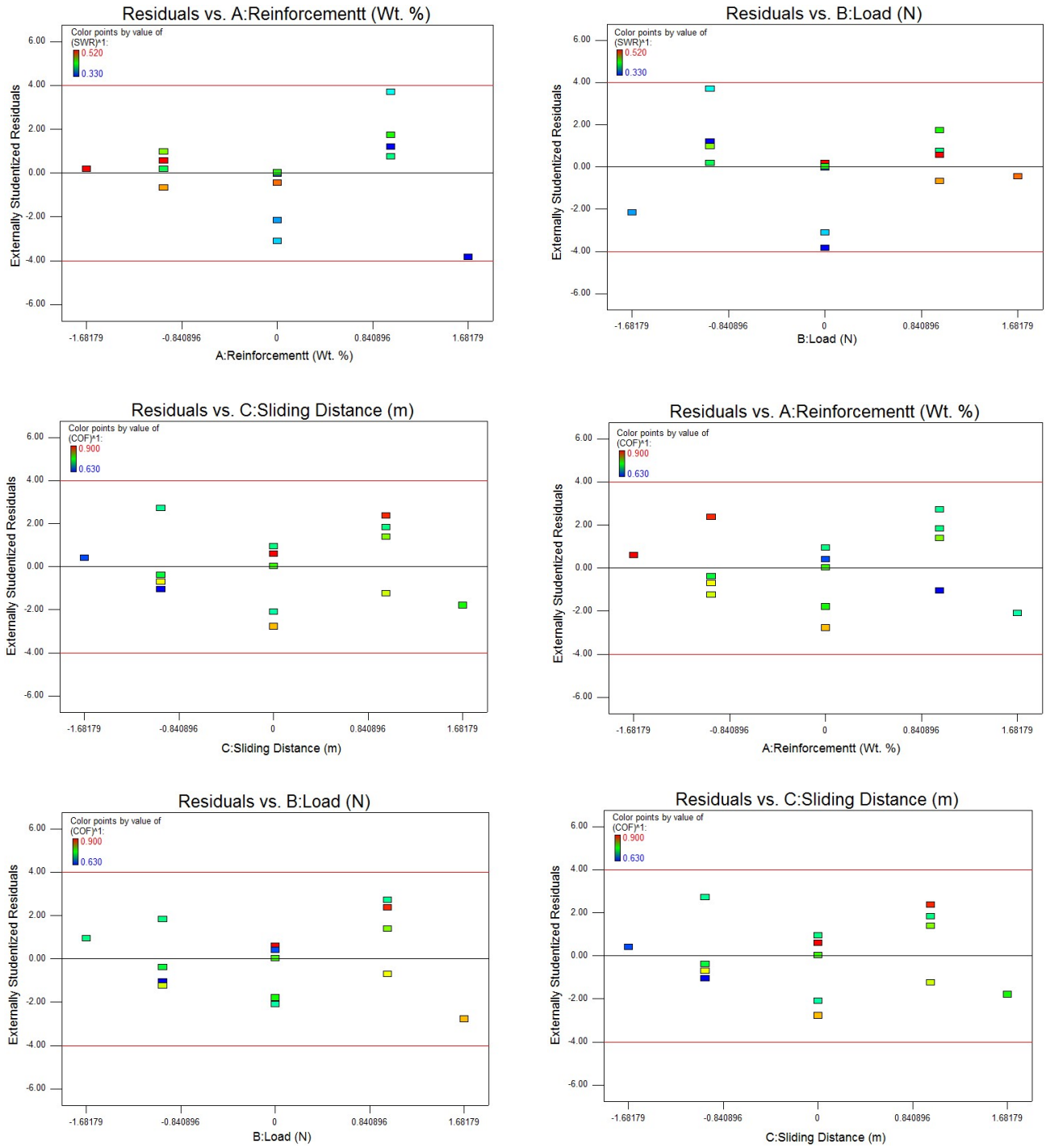

Fig. 10. Residuals plot data analysis (a-c) Specific wear rate (d-f) Coefficient of friction

coefficient of friction is also increased for base alloy because of the absence of hard asperities. The similar trend was noticed for Ti-6Al-4V / 10B_4C, the coefficient of friction is varied from 0.41, 0.43, 0.51 and 0.55 respectively. The values are clearly visualized that when compared to the base material, Ti-6Al-4V /10B_4C has minimum coefficient of friction; this is due to the presence of hard asperities (B_4C) in the matrix material. While increasing the amount of secondary particle (12 Wt. %) B_4C, again the coefficient of friction was increased because of the secondary particles has not well bond between the matrix material, due to agglomeration of the secondary particles.

4.1.2. Perturbation plot

Perturbation plot shows the effect of all the factors on a combined plot. The plot is to check the effect of all the process parameters at the centre point on the coefficient of friction is conferred in Fig. 12. It can be perceived that the coefficient of friction decreases with the increase of wt. % of B_4C (A) and this finding are well matching with [29]. It also observed that coefficient of friction is increased due to the applying load. Hence huge amount of heat was generated which increases the coefficient of friction.

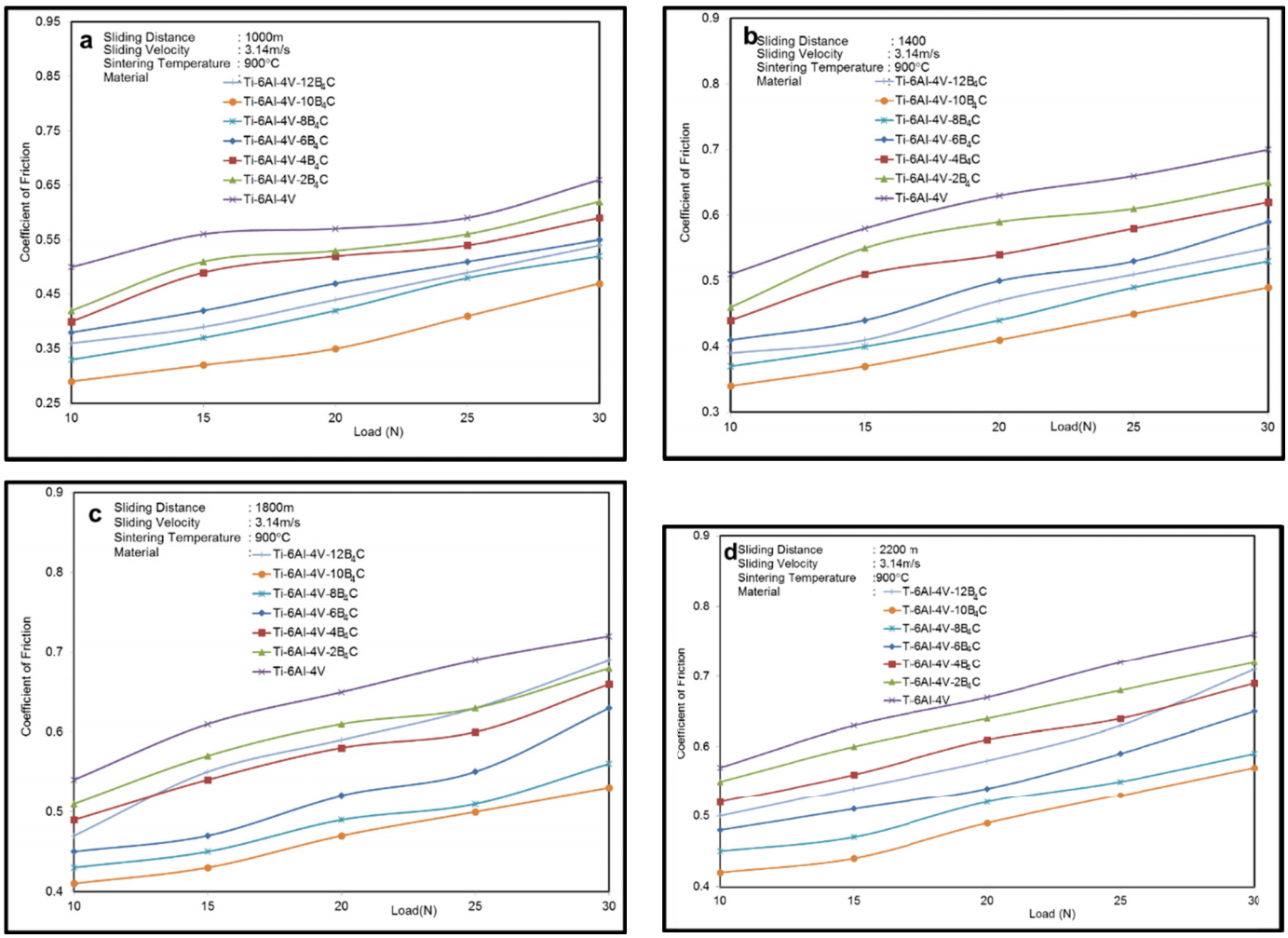

Fig. 11a-d. Coefficient of friction of various composites at various wt. % of B_4C

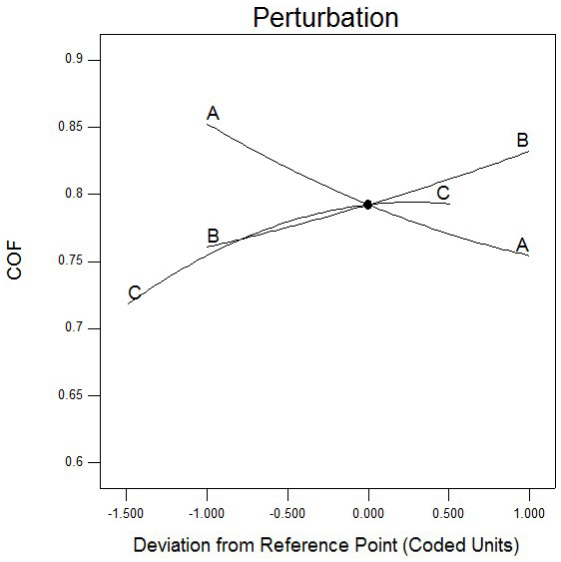

Fig. 12. Perturbation plot for coefficient of friction

4.1.3. Interaction effect

Figure 13 shows the three dimensional (3D) and two dimensional (2D) counter effect of the input factors on the coefficient of friction. Fig.13a-b indications the interaction effect of wt. % of reinforcement of B_4C and load on CoF. Fig. 13a indications the 3D surface plot. The design points were good fit with the surface plot. Fig. 13a shows the 3D surface plot of the effect of wt. % of B_4C and applied load. Fig. 13b indications the 2D counter plot in three completely different colours specifically blue for minimum value, green for average value and red for higher value. It can be established from the decreasing the coefficient of friction with increasing the wt. % of reinforcement particles due to the good bonding between the matrix and secondary particles. Fig. 13c-d indicates the interaction effect of the response plot of wt. % of reinforcement and sliding distances on coefficient of friction. Fig. 13c is the 3D plot which confirms that the coefficient of friction is decreased with increasing the wt. % of secondary particles, and further noticeable that the effect of coefficient of friction is increasing while increasing the sliding distances. Fig. 13d indications three different colours namely blue for minimum value, green for average value and red for higher value. Minimum coefficient of friction is obtained at lower sliding distances and higher wt. % of B_4C reinforced. In the other region the coefficient of friction is nominal. Fig. 13e-f shows the interaction effect of 3D response surface plot of load and sliding distance on CoF. It indicates that the minimum spe-

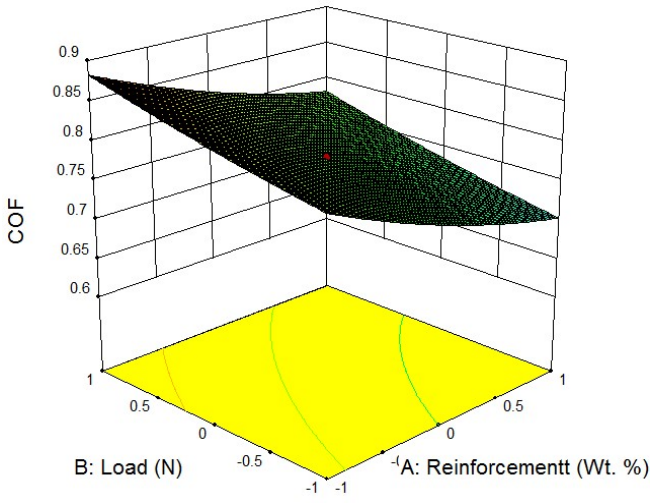

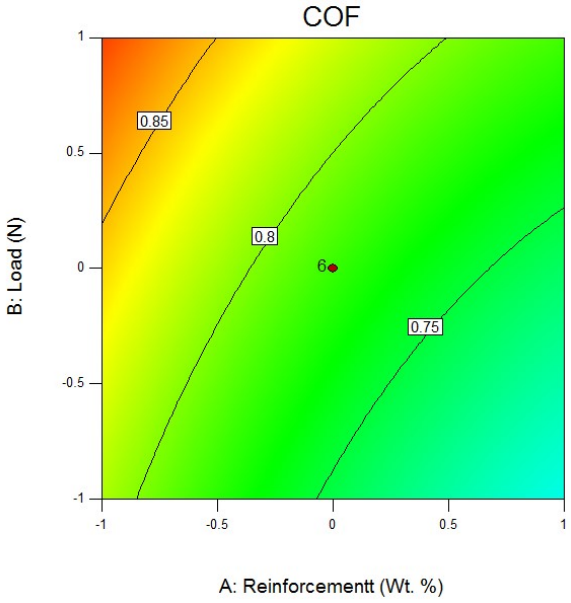

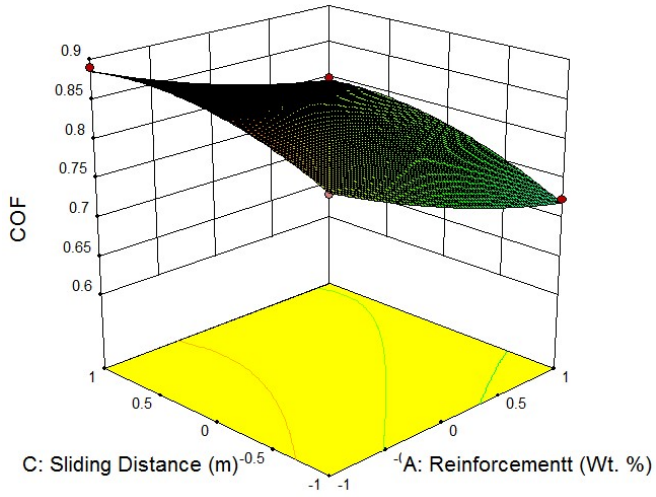

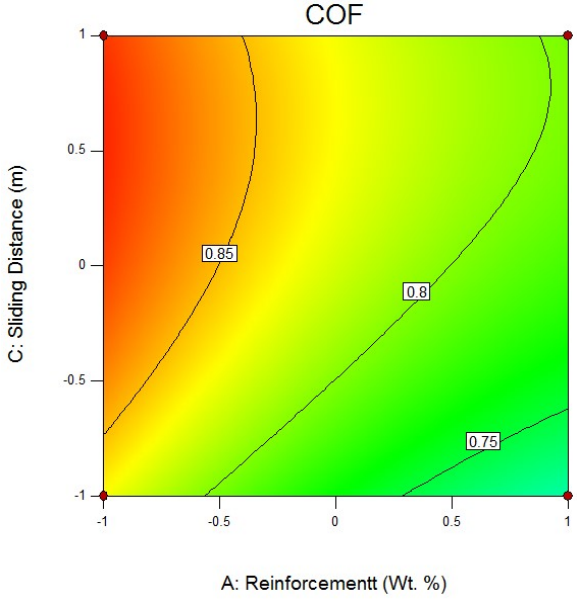

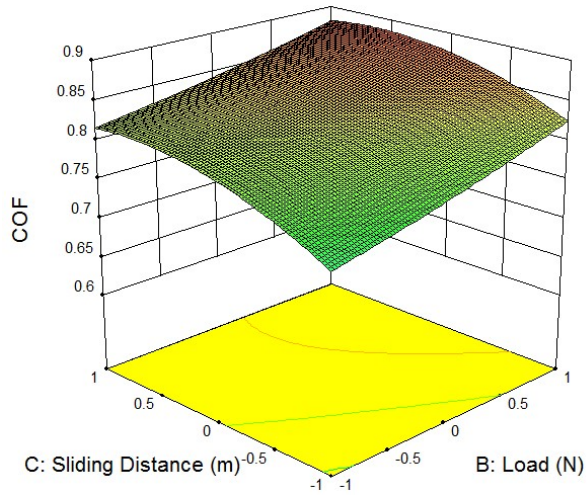

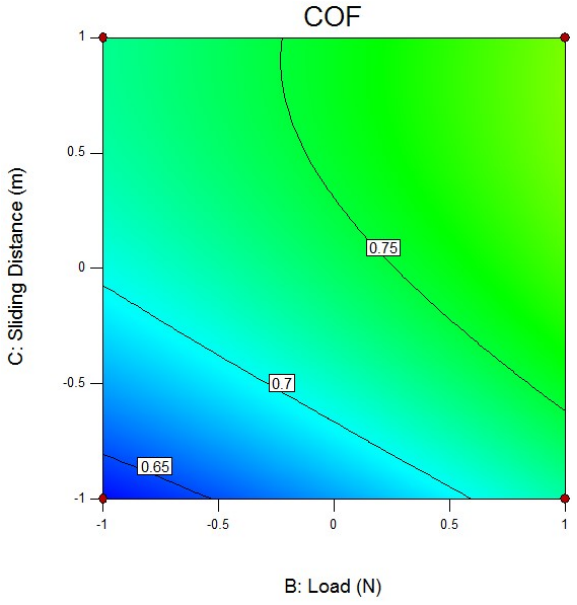

Fig. 13a-f. Interaction plot for coefficient of friction (a, c and e) 3D plot (b, d and f) 2D plot

cific wear rate is obtained at a lower sliding distance and within the remaining regions its nominal and also the design points are perfectly fit well within the plots.

4.1.4. Box plot

Figure 14 shows the box plot for Coefficient of Friction with a three process parameter design or Placket-Burman designs. From the figure it is revealed that the predicted values for each factor level combinations fit the entire model. Hence the coefficient of friction is minimum whereas increasing the Wt. % of reinforced particles and therefore the design points are perfectly fit well within the plots.

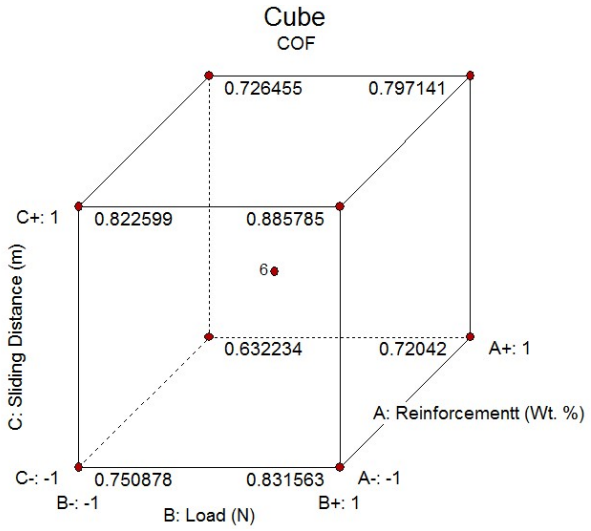

Fig. 14. Box plot for coefficient of friction

4.1.5. Analysis of variance for coefficient of friction

The significance of the developed model was analysed using ANOVA technique. The determination coefficient (R^2) indicates the goodness of fits for the developed model. The determination coefficient of less than 5% of the total variations are not explained by this model. The value of the adjusted determination coefficient (adjusted R^2) is also high, indicating a high significance of the model. The ANOVA result of the coefficient of friction is shown in table 4, which describes that the predictability of the developed model for coefficient of friction is at 99% confidence level, because the P is <0.0001. The P-value is less than <0.0001 indicating that the model is statistically significant.

4.2. Effect of specific wear rate on sliding distance

Fig. 15(a-d) shows the specific wear rate of Ti-6Al-4V -B_4C composite under different experimental conditions. Experiments were done in a disk of 120 mm diameter which rotates at a constant velocity of 3.14 m/s. A load variation between of 10-30 N was applied with a step size of 5 N. Sliding distance is varied from 1000-2200 m with an increment of 400 m at each step [24-28].

While increasing in the presence of B_4C content in the Ti-6Al-4V matrix, it is observed that a decrease in the specific wear rate, confirms the composite's effect in wear property of the base material. If dispersion of B_4C in the matrix material gets increased, the base material possesses high strength at room temperature. This is due to the fact of hard asperities have penetrated into the soft matrix material. Wear resistance of a material can be judged through two specific parameters evolved during wear testing like material weight loss and the coefficient of friction. As the hard B_4C asperities are reinforced in the soft matrix material, the wear rate decreases. This enhances the materials hardness in the ceramic phase.

From Fig. 15a-d, it is clearly shown that by increasing the load the specific wear rate is also increased. It is also evidence that, by adding hard asperities (B_4C) the specific wear rate decreases from $0.50*10^{-4}$ mm^3/N-m to $0.32*10^{-4}$ mm^3/N-m, at 30 N load under 1000 *m* sliding distance. The similar trend was noticed for other sliding distances. While sliding distance further increased from 1000 to 2200 m, the oxide transfer layer

TABLE 4

ANOVA result for coefficient of friction

Source	Sum of squares	DOF	Mean squares	F-value	P-value	Remarks
A: B_4C Content	0.087	1	$9.667E^{-003}$	687.25	<0.0001	Significant
B. Applied load	0.037	1	0.037	2607.34	<0.0001	Significant
C: Sliding distance	0.020	1	0.020	1390.41	<0.0001	Significant
AB	0.019	1	0.019	1337.12	<0.0001	Significant
AC	$2.81E^{-005}$	1	$2.813E^{-005}$	2.00	0.1877	Not Significant
BC	$2.53E^{-004}$	1	$2.531E^{-004}$	18.00	0.0017	Significant
A^2	$1.53E^{-004}$	1	$1.531E^{-004}$	10.89	0.0080	Significant
B^2	$1.78E^{-003}$	1	$1.785E^{-003}$	126.92	<0.0001	Significant
C^2	$2.37E^{-004}$	1	$2.375E^{-004}$	16.88	0.0021	Significant
Residual	$1.40E^{-004}$	10	$1.407E^{-005}$	—	—	—
Lack of fit	$1.40E^{-004}$	5	$2.813E^{-005}$	—	—	—
Pure error	0.000	5	—	—	—	—
Cor Total	0.087	19	—	—	—	—

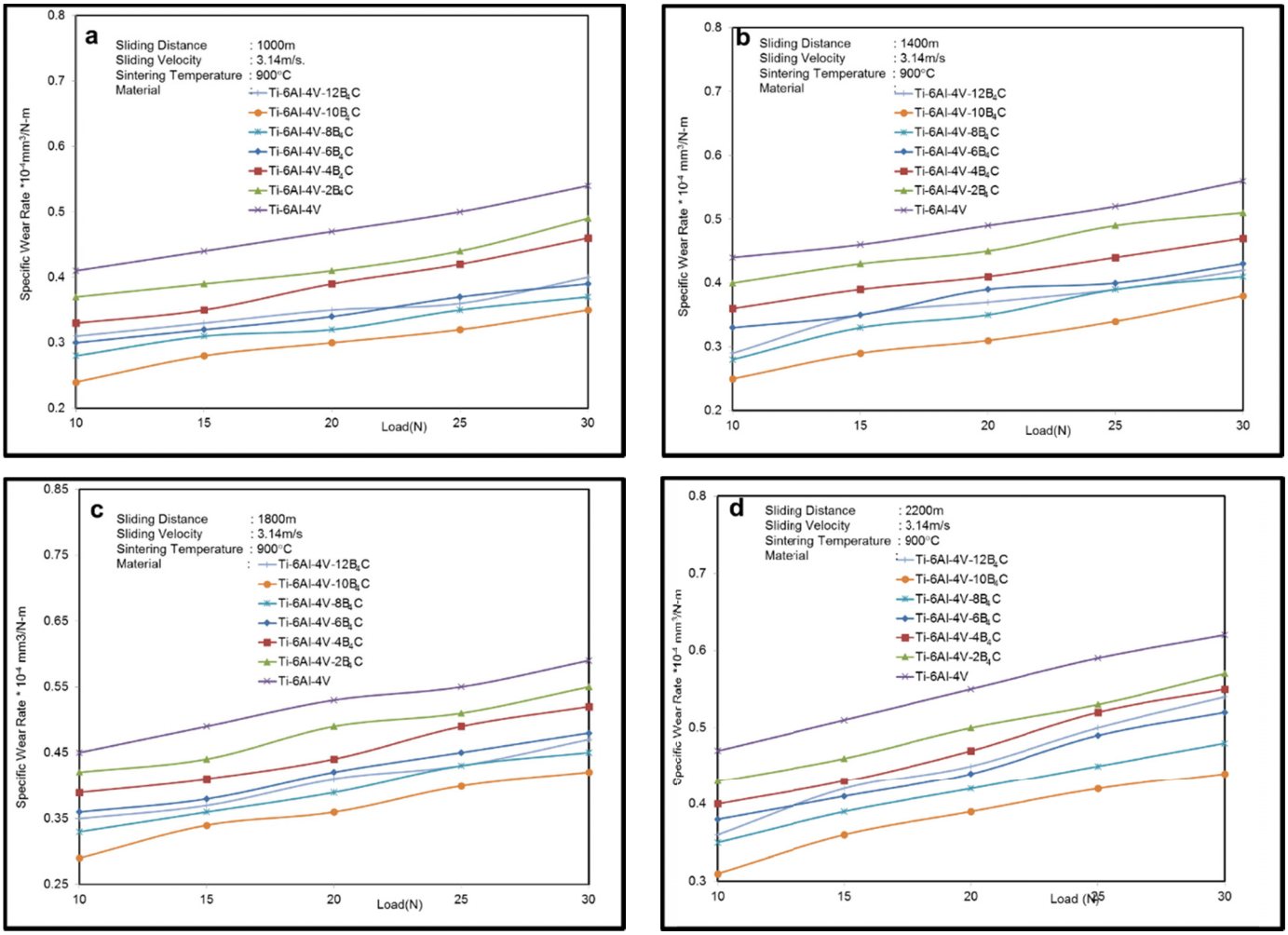

Fig. 15a-d. Specific wear rate of various composites at various wt. % of B_4C

was formed on the sliding surfaces. In the other words, the oxide transfer layer plays a vital role in friction and wear behaviour of the composites under un-lubricated sliding conditions. The oxide transfer layer prevents the direct metallic contact between the Ti-6Al-4V / B_4C composite and the steel counterpart. Adhesion between the oxide transfer layer and steel counter face is normally lower. It was concluded from the above discussion that the formation of oxide transfer layer, reduces the specific wear rate. However, the specific wear rate was determined by weight loss method, it is varied from $0.57*10^{-4}$ mm^3/N-m to $0.39*10^{-4}$ mm^3/N-m for 30 N load 2200 m sliding distance. Hence it was perceived that the wear resistance of Ti-6Al-4V /10B_4C was better than the other composites, due to the addition of ceramic B_4C phase to the Ti- 6Al-4V matrix material. Further, increasing the amount of hard asperities (12 Wt. %) B_4C, the specific wear rate has been increased irrespective of the B_4C agglomeration.

4.2.1. Perturbation plot

Perturbation plot to compare the effect of all the process parameters at the centre point on the specific wear rate is conferred in Fig. 16. From the plot, it is revealed that the SWR is decreased with the increase of wt. % of B_4C (A). Specific wear rate increases with increasing the applied load (B) and sliding distances (C) and it in good agreement with the [29-30].

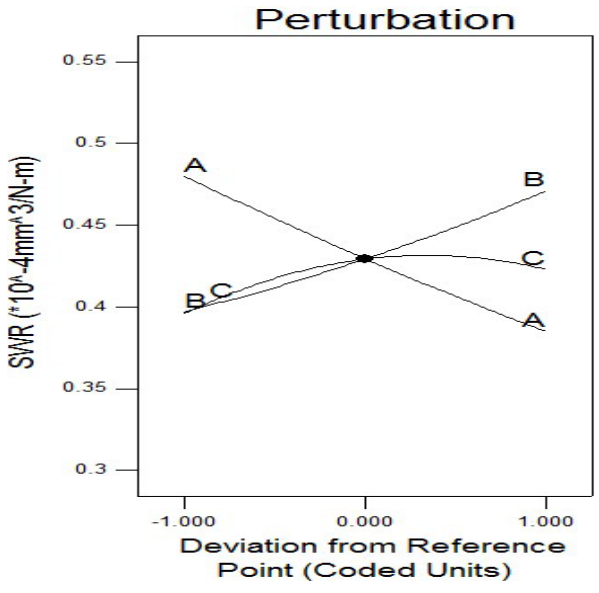

Fig. 16. Perturbation plot for specific wear rate

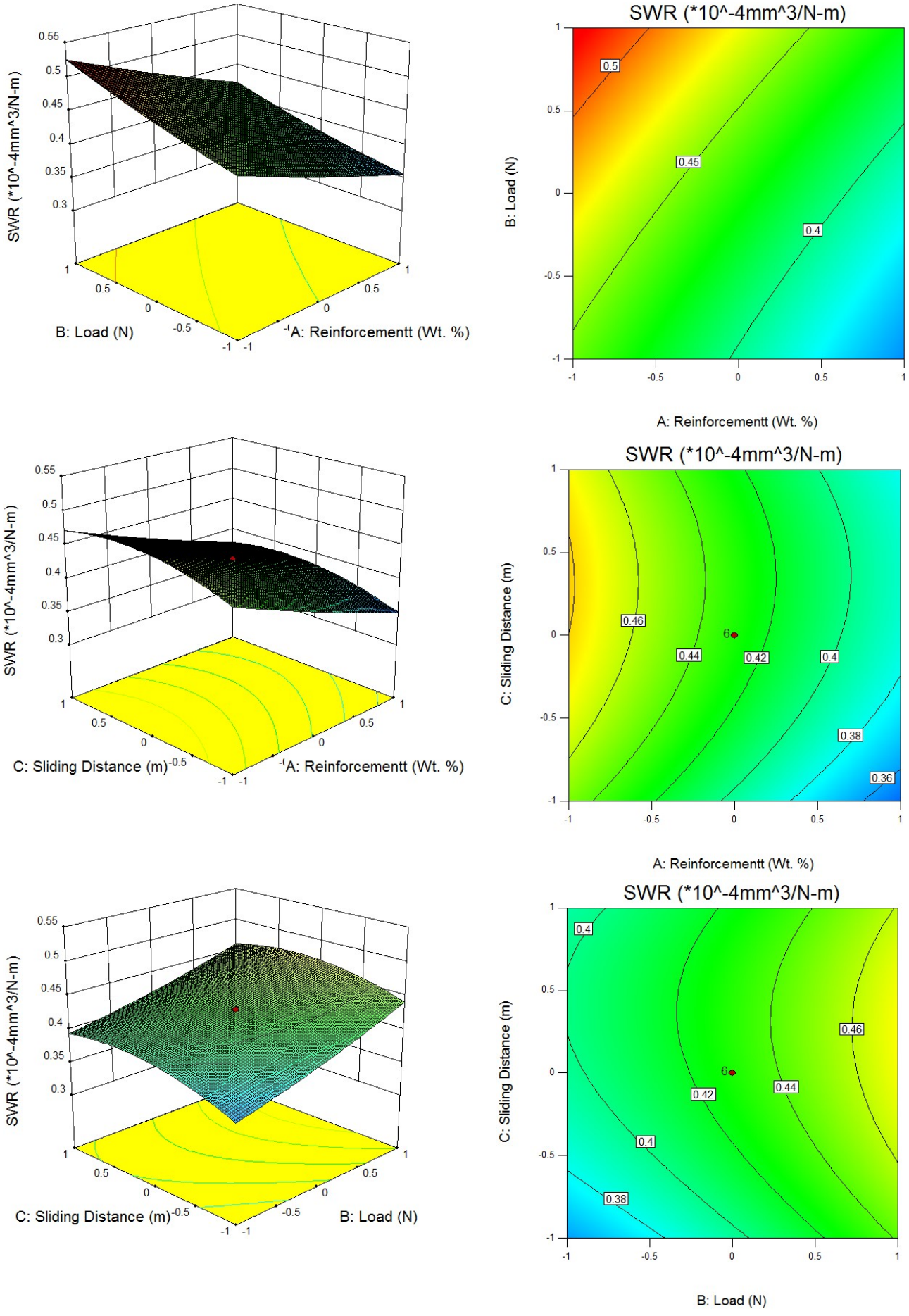

Fig. 17a-f. Interaction plot for specific wear rate (a, c and e) 3D plot (b, d and f) 2D plot

4.2.2. Interaction effect

Figure 17 shows the three dimensional (3D) and two dimensional (2D) counter plot of the factors on the specific wear rate. 3D and 2D interaction plot (Fig. 17a,b) illustrate the influence of B_4C and load on specific wear rate. Fig. 17a shows the 3D surface plot, which indicates that specific wear rate decreases with increase in the wt. % of B_4C. If dispersion of B_4C in the matrix material gets increases, the base material possesses high strength at room temperature. This is due to the fact that hard asperities have been penetrated in the soft matrix material. Wear resistance of a material can be judged through two specific parameters evolved such as material weight loss and the coefficient of friction. As the hard B_4C asperities are reinforced in the soft matrix material, the wear rate decreases. This enhances the materials hardness in the ceramic phase. This effect can be clearly noticed with the effect of 2D contour plot in three totally different colours namely, blue for minimum value, green for average value and red for higher value. The interaction effect of wt. % of B_4C and sliding distances on specific wear rate is shown in Fig. 17c,d. It found that the specific wear rate is decreased with increasing wt. % of B_4C and decreasing sliding distance. While adding B_4C, the ultra-fine B_4C particles are well bonded with the matrix materials, which reduces the wear during sliding. 2D contour plot shows in three totally different colours namely, blue for minimum value, green for average value and red for higher value. Composites underwent more sliding distance possess high specific wear rate and leads to the minimal chance for the delamination wear on the specimen.

Fig. 17e,f indicates the interaction effect of 3D response surface plot of load and sliding distance on specific wear rate. It reveals that the specific wear rate is moderately decreased with increasing the sliding distances. Fig. 17f is the 2D contour plot. It indicates the minimum specific wear rate is attained at a lower sliding distance and also the remaining region it's nominal. No red regions are identified which means that no higher specific wear rate regions are attained. Minimum specific wear rate is attained at lower sliding distance region. The specific wear rate is moderate at the rest of the region.

4.2.3. Box plot

Figure 18 shows the box plot for SWR with a three process parameter design or Placket-Burman design. It illustrated that the forecasted values for each factor level combinations are adequate throughout the entire model. Hence, the specific wear rate is minimum and decreases with increasing Wt. % of reinforced particles. Hence the design points are perfectly fit well with in the plots.

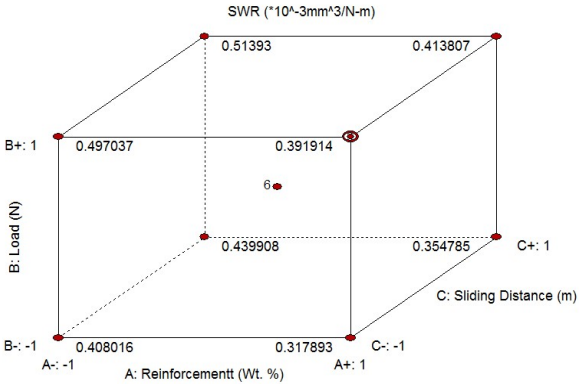

Fig. 18. Box plot for specific wear rate

4.2.4. Analysis of variance for specific wear rate

The ANOVA result for the specific wear rate is shown in table 5, which directs that the predictability of the model for specific wear rate is at 99% confidence interval. The forecast response fit well with those of experimentally attained responses. The P-value of the specific wear rate is <0.0001, indicating that the developed model is statistically significant.

4.2.5. Validation

Fig. 19 indicates the relationship between the predicted and experimental values of the specific wear rate and coefficient of

TABLE 5

ANOVA result for specific wear rate

Source	Sum of squares	DOF	Mean squares	F-value	P-value	Remarks
A: B_4C Content	0.059	1	$6.555E^{-003}$	20.58	< 0.0001	Significant
B. Applied load	0.031	1	0.031	96.97	< 0.0001	Significant
C: Sliding distance	0.019	1	0.019	58.72	< 0.0001	Significant
AB	$2.46E^{-003}$	1	$2.469E^{-003}$	7.75	0.0193	Significant
AC	$1.12E^{-004}$	1	$1.125E^{-004}$	0.35	0.5655	Not Significant
BC	$1.25E^{-005}$	1	$1.25E^{-005}$	0.039	0.8470	Not Significant
A^2	$1.12E^{-004}$	1	$1.12E^{-004}$	0.35	0.5655	Not Significant
B^2	$1.32E^{-004}$	1	$1.32E^{-004}$	0.42	0.5329	Not Significant
C^2	$3.36E^{-004}$	1	$3.32E^{-004}$	1.04	0.3310	Not Significant
Residual	$3.16E^{-003}$	10	$3.18E^{-004}$	17.99	0.0017	Significant
Lack of fit	$3.18E^{-003}$	5	6.37^{E-004}	—	—	—
Pure Error	0.000	5	0.000	—	—	—
Cor Total	0.062	19	—	—	—	—

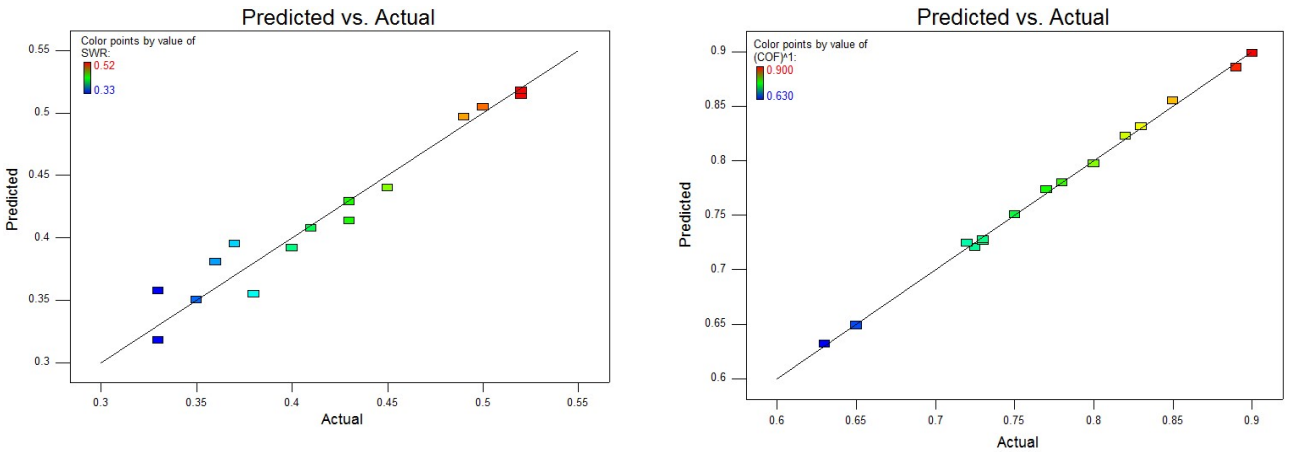

Fig. 19. Relationship between the experimental and predict id (a) specific wear rate (b) coefficient of friction

friction. From the figure, the developed model are acceptable and the predicted values are in good agreement with the measured data. Compared to the measured value with the predicted value, it is detected that there is some deviation, however the deviation is nominal. Hence the equation predicts the specific wear rate as well as coefficient of friction with minimum error.

4.2.6. Optimization

The optimal parameter of the SWR and CoF is to be established from the results of the RSM over lay plot. It is observed from the plots that the lowest point of SWR and CoF is 10% B_4C reinforcement for any values of applied load, and sliding distance. Thus, it can be concluded that the optimal B_4C reinforcement content is around 10%. Applied load and sliding distance are the most influencing parameters respectively. At the optimal level of the applied load and sliding distance, an

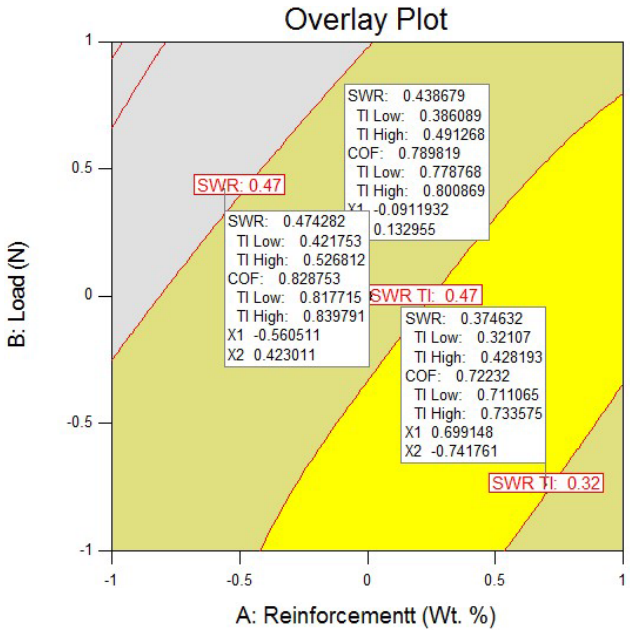

Fig. 20. Overlay plot for SWR and CoF

increase within the sliding distance makes the increase of SWR and CoF. The effect of applied load is much superior, compared to the sliding distance. From the Fig. 20, it is inferred that the optimal SWR ($0.4292*10^{-4}$ mm^3/N-m) and CoF (0.7803) for the prepared composites.

4.3. Worn surface analysis

The SEM analysis of the worn surface of the Ti-6Al-4V/B_4C composites is shown in Fig. 21a-f. Fig. 21a shows the SEM image of Ti-6Al-4V matrix material. It has been clearly visualized by severe adhesive wear in the composite. Furthermore, it also shows that ploughing of metals appears parallel to the sliding direction. When the disc contacts the sample, the hard counter steel body presses the Ti-6Al-4V specimen, so that the friction coefficient and wear loss become high. The ploughing of metal is possible due to the direct metal contact between the specimen and steel counter disc, this is exerted by the hardened wear debris from Ti-6Al-4V. Fig. 21b-g shows the worn surface of Ti-6Al-4V matrix with 2, 4, 6, 8, 10 and 12 wt. % of B_4C. It can relatively be than that of the Ti-6Al-4V matrix. Because, the hard ceramic particles are much harder than the Ti-6Al-4V matrix and thus, better wear resistance can be obtained. Moreover, with increase in the B_4C content, the worn surfaces of the composites become smoother.

The B_4C particles can act as a shielding, and which protect the Ti-6Al-4V matrix from the plastic deformation and foremost to the reduced micro ploughing and thus lower wear rate of the composites. Hence the wear resistance of the composites is better than that of the Ti-6Al-4V matrix. As the B_4C content increases, the penetration of the ceramic particles is enriched, leading to the better wear resistance. It can also be seen from the Fig. 21a-d, that the wear rate of the Ti-6Al-4V matrix and composites increases with increasing the load. While the applied load increases from 10 N to 30 N, the worn surface of the Ti-6Al-4V matrix becomes rougher, as shown in Fig. 21a. While incorporated B_4C to the Ti-6Al-4V matrix the worn surface becomes smoother, as evident in Fig. 21b-g. During the wear test the applied load

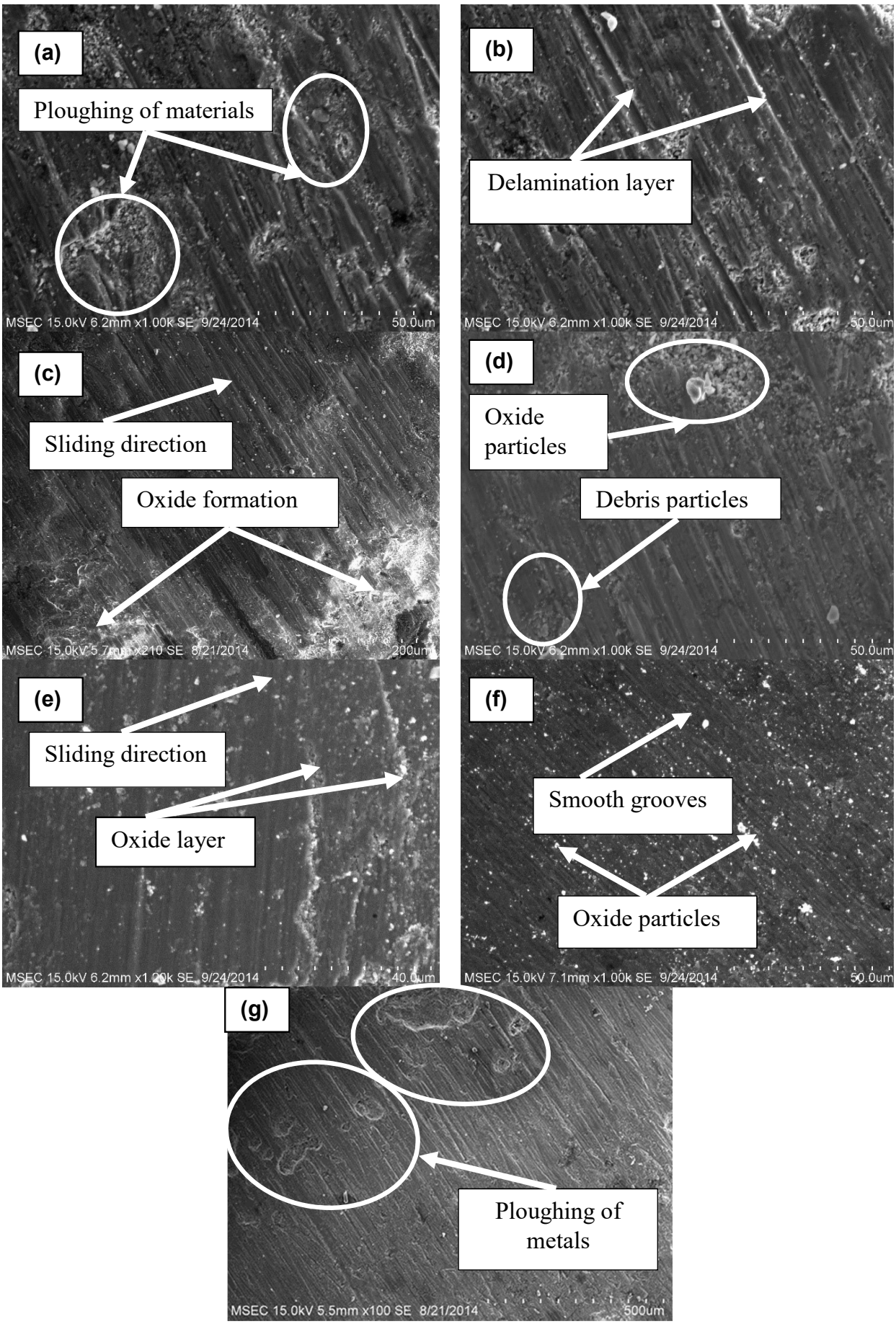

Fig. 21a-f. SEM micrograph of a worn surface after wear test of various composites (a) Ti-6Al-4V matrix (b) Ti-6Al-4V / $2B_4C$ (c) Ti-6Al-4V / $4B_4C$ (d) Ti-6Al-4V / $6B_4C$ (e) Ti-6Al-4V / $8B_4C$ (f) Ti-6Al-4V / $10B_4C$ and (g) Ti-6Al-4V / $12B_4C$ composites

is relatively large, the ceramic particles are squeezed from the Ti-6Al-4V matrix, and acts as a shielding throughout the test. Figure 21f shows the worn surface of the 10 wt. % of B_4C reinforced with Ti-6Al-4V matrix which is completely protected by the hard ceramic particle, it is also noted that the smooth grooves were formed in the composites. Moreover, the addition of 10 wt. % of B_4C particles to the Ti-6Al-4V matrix considerably increase the hardness of the composite and resulted in a reduction of the plastic deformation of matrix, in this case the wear loss of the composite is reduced, while compared to the other composites. It is strongly inferred that the wear rate can be reduced gradually with addition of B_4C. The specific wear rate has also been increased further with the reinforcing of 12 Wt. %. B_4C particles. This could be inferred from the above graphs and also from the Fig. 21g.

4.4. Wear debris analysis

During the wear testing, the wear debris was analysed for the load of 30 *N* and sliding distances of 2,200 m. The detailed micro structural investigation of the wear of Ti-6Al-4V matrix and its composites was carried out using SEM. Figure 22(a-d) shows the SEM image of the wear debris of Ti-6Al-4V matrix and Ti-6Al-4V / (2-12) wt. % of B_4C composite. Fig. 22a shows the SEM image of Ti-6Al-4V matrix and reveal very thick layer debris particles were observed and this is correlated with the more specific wear rate, because of the direct metal contact between the specimen and the steel counter disc. Also noted that for the highest load, the formation of tribo layer and its area of coverage also increased when compared to all other composites. Large sizes of wear debris particles are observed and this correlates with the more wear loss in Ti-6Al-4V matrix. This is because of the absence of B_4C content. Fig. 22b-d shows the SEM image of the Ti-6Al-4V / (2-12) wt. % of B_4C composites. Finer debris particles were progressed due to the presence of hard asperities in the composites, which turned out to be a protective layer to the specimen. The oxide layer formed during the sliding acts as a barrier to the specimen and counter disc. Moreover, while increasing the B_4C, the hardness of the composite was enhanced [23-24].

5. Conclusion

Ti-6Al-4V matrix incorporated with B_4C particles were prepared through P/M technique in order to enhance the mechanical properties of wear resistance, coefficient of friction and hardness.

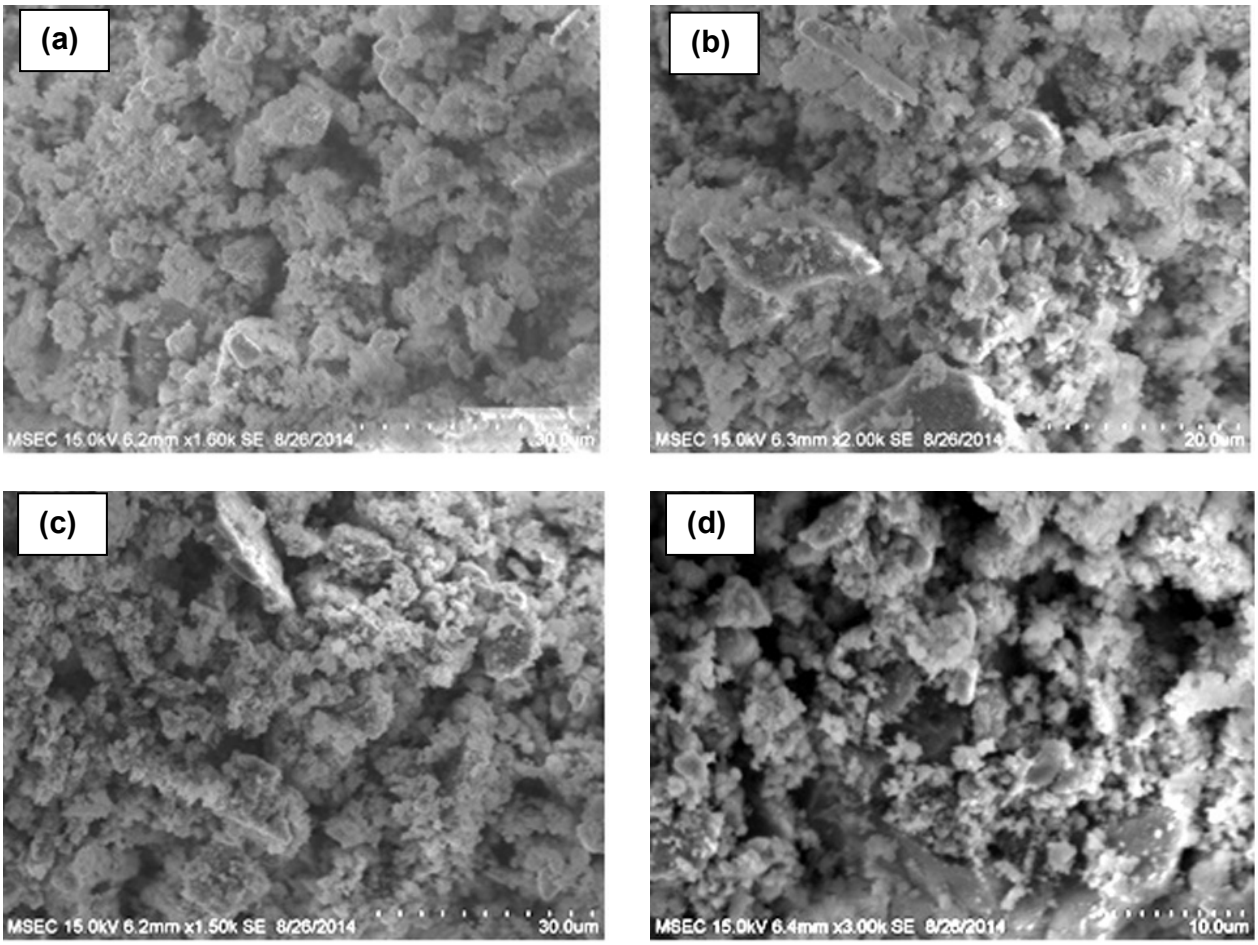

Fig. 22a-d. SEM micrograph of a wear debris particles after wear test of various composites (a) Ti-6Al-4V matrix (b) Ti-6Al-4V /4B_4C (c) Ti-6Al-4V /8B_4C (d) Ti-6Al-4V /12B_4C composites

The wear resistance, coefficient of friction and hardness increase with the volume fraction (10 Wt. %) of milled B_4C powder. Furthermore, while increasing the volume fraction (12 Wt. %) of B_4C the hardness, specific wear rate and coefficient of friction were decreased significantly because of agglomeration of the secondary particles. It evidently indicates that the B_4C particles in the Ti-6Al-4V matrix are more effective in resisting wear rate at room temperature condition. RSM central composite design method is efficiently used to develop the model and is used to decrease the experiments in future. ANOVA is used to check the suitability of the developed model. Good agreement exists between the experimental and predicted value. The model has good adequacy, which can be used to find out the value with less error. Analysis of overlay plots predict that the increase in B_4C reinforcement content reduces SWR and CoF to about 10%B_4C, and beyond this the wear loss has the propensity to increase. Thus, the optimal wt.% of B_4C reinforcement content can be about 10% for any value of applied load and distance. The optimal SWR ($0.4292*10^{-4}$ mm^3/N-m) and CoF (0.7803) were determined using overlay plot.

REFERENCES

[1] H. Abkowitz, M.S. Abkowitz, D. David, Effect of tungsten additions on the mechanical properties of Ti-6Al-4V, Materials Science Engineering A **396**, 99-106 (2005)

[2] M. Kobayashi, K. Funami, S. Suzuki, C. Ouchi, Manufacturing process and mechanical properties of fine TiB dispersed Ti-6Al--4V alloy composites obtained by reactive sintering, Materials Science and Engineering A **243**, 279-284 (1998).

[3] R.-H. Hu, J.-K. Lim, Hardness and wear resistance improvement of surface composite layer on Ti-6Al-4V substrate fabricated by powder sintering, Materials and Design **31**, 2670-2675 (2010).

[4] A. Mahboubi, S. Soufiani, M.H. Enayati, F. Karimzadeh, Mechanical alloying behaviour of Ti-6Al-4V residual scraps with addition of Al_2O_3 to produce nanostructured powder, Materials and Design **2010**, 31, 3954-3959 (2010).

[5] M. Dewidar, Microstructure and mechanical properties of biocompatible high density Ti-6Al-4V/W produced by high frequency induction heating sintering. Materials and Design **31**, 3964-3970 (2010).

[6] E.M. Sharifi, F. Karimzadeh, M.H. Enayati, Fabrication and evaluation of mechanical and tribological properties of boron carbide reinforced aluminium matrix nanocomposites, Materials and Design **32**, 3263-3271 (2011).

[7] Z.-Q. Yan, F. Chen, T.-X. Cai, J. Yin, Influence of particle size on property of Ti-6Al-4V alloy prepared by high-velocity compaction, Transactions of Nonferrous Metals **23**, 361-365 (2010).

[8] C.Y. Tang, C.T. Wong, L.N. Zhang, In situ formation of Ti alloy/TiC porous composites by rapid microwave sintering of Ti-6Al--4V/MWCT powder, Journal of alloys and compounds **557**, 67-72 (2013).

[9] I. Montealgere Melendez, E. Neubauer, P. Angerer, Influence of nano-reinforcements on the mechanical properties and microstructure of titanium matrix composites, Composites Science and Technology **71**, 1154-1162 (2011).

[10] C. Poletti, M. Balog, T. Schubert, Production of titanium matrix composites reinforced with SiC particles, Composites Science and Technology **68**, 2171-2177 (2008).

[11] H. Rastegri, S.M. Abbasi, Producing Ti-6Al-4V/TiC composite with superior properties by adding boron and thermo-mechanical processing, Materials Science & Engineering A **564**, 473-477 (2013).

[12] Y.L. Xi, D.L Chai, W.X. Zhang, J.E. Zhou, Ti-6Al-4V particle reinforced magnesium composite by powder metallurgy, Materials letters **59**, 1831-1835 (2005).

[13] M. Anandajothi, S. Ramanathan, V. Ananthi, P. Narayanasamy, Fabrication and characterization of Ti6Al4V/TiB_2-TiC composites by powder metallurgy method, Rare Metals **36** (10), (2017).

[14] T.M.T. Godfrey, A. Wisbey, P.S. Goowin, C.M. Bagnall, C.M. Ward-Close, Microstructure and tensile properties of mechanically alloyed Ti-6Al-4V with boron addition, Materials Science Engineering **282**, 240-250 (2000).

[15] S.J. Zhu, D. Mukherji, W. Chen, Z.G. Wang, R.P. Wahi, Steady state creep behaviour of TiC particulate reinforced Ti-6Al-4V composite, Materials Science Engineering A **256**, 301-307 (1998).

[16] N. Atiqah, M. Aziz, R. Yunus, U. Rashid, A.M. Syam, Application of response surface methodology (RSM) for optimizing the palm-based pentaerythritol ester synthesis, Industrial Crops and Products **62**, 305-312 (2014).

[17] S.C. Vettivel, N. Selvakumar, R. Narayanasamy, N. Leema, Numerical modelling, prediction of Cu–W nano powder composite in dry sliding wear condition using response surface methodology, Materials & Design **50**, 977-996 (2013).

[18] Z.-R. Yang, Y. Sun, X.-X. Li, S.-Q. Wang, Dry sliding wear performance of 7075 Al alloy under different temperatures and load conditions, Journal of Rare Metals, (2015).

[19] N. Selvakumar, T. Ramkumar, Effect of high temperature wear behaviour of sintered Ti-6Al-4V reinforced with nano B_4C particles, Transactions of the Indian Institute of Metals **69** (6), 1267-1276 (2016).

[20] P. Narayanasamy, N. Selvakumar, Effect of hybridizing and optimization of TiC on the tribological behavior of Mg-MoS_2 composites, ASME Journal of Tribology **139** (5), (2017); 051301-311.

[21] N. Selvakumar, P. Narayanasamy, Optimization and effect of weight fraction of MoS_2 on the tribological behaviour of Mg--TiC-MoS_2 hybrid composites, Tribology Transactions Taylor & Francis Publications **59** (4), 733-747 (2016).

[22] N. Selvakumar, P. Radha, R. Narayanasamy, M.J. Davidson, Prediction of deformation characteristics of sintered aluminium preforms using neural networks, Modelling and Simulation in Materials Science and Engineering **12** (4), 611-620 (2004).

[23] N. Selvakumar, T. Ramkumar, Effect of Particle Size of B_4C Reinforcement on Ti-6Al-4V Sintered Composite Prepared by Mechanical Milling Method, Transactions of Indian Ceramic Society **76** (1), 31-37 (2017).

[24] P. Ravindran, K. Manisekar, R. Narayanasamy, P. Narayanasamy, Tribological behaviour of powder metallurgy – processed

aluminium hybrid composites with the addition of graphite solid lubricant, Ceramic International **39**, 1169-1182 (2013).

[25] N. Selvakumar, S.C. Vettivel, Thermal, electrical and wear behaviour of sintered Cu-W nanocomposite, Materials and Design **46**, 16-25 (2013).

[26] Zhang Zhi-Xiao, DU Xian-Wu, Wang Wei-Min, Fu Zheng-Yi, WangHao, Preparation and Sintering of High Active and Ultrafine B_4C-SiC Composite Powders, Journal of Inorganic Material **29**, 185-190 (2014).

[27] Y. Li, F. Zhang, T.-T. Zhao, M. Tang, Y. Liu, Enhanced wear resistance of NiTi alloy by surface modification with Nb ion implantation, Journal of Rare Metals **33** (3), 244-248 (2014).

[28] P. Narayanasamy, N. Selvakumar, P. Balasundar, Effect of hybridizing MoS_2 on the Tribological behaviour of Mg-TiC Composites, Transactions of the Indian Institute of Metals **68** (5), 911-925 (2015).

[29] A.K. Parida, B.C. Routara, R.K. Bhuyan, Surface roughness model and parametric optimization in machining of GFRP composite: Taguchi and Response surface methodology approach, Materials Today Proceedings **2**, 3065-3074 (2015).

[30] P. Ravindran, K. Manisekar, P. Narayanasamy, N. Selvakumar, R. Narayanasamy, Application of factorial techniques to study the wear behaviour of Al hybrid composites with Graphite Addition Elsevier publications, Materials and Design **39** (7), 42-54 (2012).